https://doi.org/10.5194/egusphere-2026-4262
Preprint. Discussion started: 31 August 2026

Ent Köppen-Geiger v1.0, a software tool for generating Earth System Model global vegetation boundary conditions for alternative climates

Nancy Y. Kiang[a*], Cheuk Yin James Lui[b], Linda Sohl[b], Scott Guzewich[c]

[a]NASA Goddard Institute for Space Studies (GISS), c/o Office of Research Initiatives and Development, Low Library, Room 409A, Columbia University, 535 West 116th Street, Mail Code 4312, New York, NY 10027 U.S.A., Nancy.Y.Kiang@nasa.gov
[b]Autonomic Integra LLC, c/o Office of Research Initiatives and Development, Low Library, Room 409A, Columbia University, 535 West 116th Street, Mail Code 4312, New York, NY 10027 U.S.A., james.lui@nasa.gov, les14@columbia.edu
[c]NASA Goddard Space Flight Center (GSFC), Mail Code 699, Greenbelt, MD, 20771, U.S.A., scott.d.guzewich@nasa.gov

**Correspondence to*: Nancy Y. Kiang (Nancy.Y.Kiang@nasa.gov)

Abstract. We used the Köppen-Geiger biome-climate classification scheme to produce a software tool for predicting global maps of vegetation boundary conditions (VBCs) (soil and plant type cover fractions, canopy heights, annual maximum and monthly leaf area index) for Earth System Model (ESM) simulations of vegetation-atmosphere coupling in alternative climates. A modern Köppen-Geiger biome map derived from observed mean monthly climatology (2001-2010) was used as a mask to characterize statistics of contemporaneous satellite-observed VBCs categorized into the 12 plant functional types (PFTs) of the Ent Terrestrial Biosphere Model. A lookup table (LUT) of these VBCs was then constructed tabulating VBCs for each Köppen-Geiger class. For paleo-vegetation back to the Cretaceous, additional algorithms were designed to replace grasses and deciduous trees with time-relevant cover types. To evaluate the efficacy of the lookup table and paleo-vegetation algorithms, we conducted both modern and Cretaceous climate simulations with the NASA Goddard Institute for Space Studies ESM ModelE-2.1 and its generalized planetary version. Climate simulations for the modern, 2001-2010, using the LUT-generated VBCs showed simulated climate to have no significant difference from using the original satellite-derived VBCs. For the Cretaceous Thermal Maximum, given a preliminary simulated climate having bare soil for the land surfaces, predicted maps of cover types largely capture the vegetation type patterns compared to fossil reconstructions, while reflecting a high latitude cold bias of the simulated climate. The "Ent Köppen-Geiger" v1.0 software tool is made available for community updates and studies with asynchronous vegetation-climate model coupling for past to future climates.

Keywords: vegetation boundary conditions, Earth System Model, paleo-vegetation, Köppen-Geiger, climate classification

1 Introduction

Climate modelling requires specification of surface boundary conditions consistent with the given climate scenario, including vegetation. For coupling with the atmosphere, the vegetation physics must at minimum account for sensible and

https://doi.org/10.5194/egusphere-2026-4262
Preprint. Discussion started: 31 August 2026

latent heat partitioning for the land surface energy balance, physics that are directly coupled with the biophysics of photosynthetic uptake of CO_2 and transpiration of H_2O vapor. Vegetation boundary conditions (VBCs) must describe the parameters for surface albedo, surface conductance, and roughness length which can range from simple paint-by-numbers prescriptions of land cover maps as in early atmospheric general circulation models (GCMs) (Hansen et al., 1983) to simulating the seasonal leaf area index and ecological dynamics of mixed canopies with variability in physiological traits and human land use (Fisher & Koven, 2020). The level of complexity in the vegetation model must be tailored to the scientific question, from broad climatological characterization (Prentice et al., 1992) to projecting the future trajectory of the carbon cycle with feedbacks between vegetation and the atmosphere (Argles et al., 2022; Friedlingstein et al., 2025; Sitch et al., 2024). How sufficiently to describe those VBCs and predict their geographic distribution remains an ongoing research challenge for modelers and observational scientists.

Vegetation is an expression of climate: the structural characteristics of a biome (mixture of vegetation types, plant densities, plant morphology, seasonality, and other properties) to first order result from structural and temporal adaptations to access the available resources of water, light, and nutrients, constrained by temperature and disturbances like windthrow, fire, and herbivory. Geographers have long developed approaches to classify biome types through mapping correlations with climate variables (Holdridge, 1947; Holdridge, 1967; Köppen, 1884; Whittaker, 1967). A process-based understanding evolved with the development of GCMs that required simulation of land surface latent and sensible heat partitioning and surface fluxes of water vapor from vegetation, developing further to include stomatal coupling with atmospheric CO_2 and carbon dynamics in dynamic global vegetation models (DGVMs), whose physics are forced by meteorological drivers, off-line or coupled with atmospheric GCMs. For such models, the representation of biome classes comprising mixed vegetation communities was superseded by the concept of physiognomic "plant functional types" (PFTs), to represent certain salient features of vegetation that could also be observed by Earth-observing satellites for mapping vegetation globally (Defries et al., 1995): growth form (herbaceous, shrub, tree), photosynthetic pathway (C3, C4), leaf shape (needleleaf, evergreen), phenology (evergreen/deciduous, annual/perennial). With these PFT distinctions, the biophysics component of state-of-the-art models requires optical and physiological properties of the PFT, and VBC variables must include cover maps, temporal leaf area index, and canopy heights to simulate canopy radiative transfer and albedo, photosynthesis, and transpiration. The limited diversity represented in these computationally intensive models can otherwise capture major distributions of their biophysical effect on climate, and it remains a major research area to improve these models in their predictions of biogeochemistry and biogeography (Fisher & Koven, 2020; Friedlingstein et al., 2025). To date, DGVMs largely can simulate well the biophysics of photosynthesis and transpiration (with some tuning) (Friend et al., 2007; Gu et al., 2000), have been little evaluated with regard to albedo prediction (Widlowski et al., 2015; Widlowski et al., 2011; Widlowski et al., 2013), do poorly in predicting phenological timing of foliage and seasonality of biophysical parameters (Friedlingstein et al., 2006; Friedlingstein et al., 2014; Piao et al., 2019; Richardson et al., 2012), have large uncertainties in carbon dynamics (Friedlingstein et al., 2014; Friedlingstein et al., 2025), and vary in their ability to predict geographic distributions of cover types (Sitch et al., 2008; Song

https://doi.org/10.5194/egusphere-2026-4262
Preprint. Discussion started: 31 August 2026

et al., 2021). Better representation of vegetation diversity remains an area of research (Ma et al., 2025; van Bodegom et al., 2014).

Not all global scale modelling studies require the full dynamics of prognostic phenology, carbon accounting, and cover change, but they still require vegetation boundary conditions (VBCs) for the simulation of biophysical surface fluxes. For the global paleoclimate and paleo-vegetation modelling community, "One of the most time consuming, and often daunting, tasks...is the production of surface boundary conditions for past time periods" (Sewall et al., 2007). Typically, paleoclimate studies rely on very broad climate reconstructions to gap-fill fossil reconstructions of vegetation maps to prescribe the VBCs (Herold et al., 2014; Pound et al., 2012; Prentice & Webb, 1998; Sewall et al., 2000; Sewall et al., 2007) to simulate the climate of the time period of interest. Often, these reconstructions will provide cover maps, while other VBCs, such as leaf area index, must be supplied by a particular model's parameterizations for the vegetation type. Studies utilizing process-based vegetation models of varying complexity to predict distributions of major biomes or PFTs tend to be driven off-line with meteorological forcings obtained from a GCM simulation of the given time period that used reconstructed VBCs (Shellito & Sloan, 2006a, 2006b). The BIOME model of Prentice et al. (1992) used a simple climate classification to predict distributions of 13 biomes rather than PFTs, based on temperature limits, cumulative chilling requirements, cumulative heating requirements, and mean soil moisture tolerances (Prentice, 2000; Prentice et al. 1992; Harrison et al. 1998). This model and its later versions have been used to provide cover protocol maps for models participating in the Paleoclimate Modelling Intercomparison Project (PMIP) for the Pliocene and Holocene (Bracconot et al. 2007) and Eocene (Herold et al., 2014). As the concept of plant functional types (PFTs) was recognized as a means to classify vegetation according to ecophysiological traits (Defries et al., 1995; Dorman & Sellers, 1989), the biome-based BIOME model was superseded by the PFT-based BIOME3 (Haxeltine & Prentice, 1996). Subsequently, BIOME4 (Kaplan et al., 2003) introduced additional tundra PFTs, and physics driven off-line to simulate surface fluxes of a daily soil water balance and monthly canopy conductance, photosynthesis, respiration, and phenology. The model uses the monthly biogeochemical quantities to rank combinations of PFTs to assign a biome for each grid cell. The latest PMIP4 protocols allowed for fully dynamic vegetation (Kageyama et al., 2018), but submitted models all prescribed vegetation distributions to simulate climate (Brierley et al., 2020). In the Eocene Modelling Intercomparison Project (EoMIP), the models adopted model-specific VBCs (Lunt et al., 2012).

Paleo-vegetation studies with fully coupled GCM-DGVMs having climate-vegetation feedbacks remain few. These require biophysics to be simulated at ~half-hourly physical time steps to produce surface fluxes to drive atmospheric circulation, with results subject to biases of both the vegetation model and the climate model. An example is use of the Organising Carbon and Hydrology In Dynamic Ecosystems (ORCHIDEE) DGVM, including fire dynamics, which could match 69% of the pixels of forest cover compared to the BIOME 6000 fossil reconstructions of the Last Glacial Maximum (LGM), compared to 84% of the forest cover under high CO_2 during the preindustrial (Chen et al., 2019). For predicting vegetation distributions, whether off-line or coupled, there are challenges due to weaknesses of DGVMs as mentioned earlier, as well as differences in vegetation types relevant to the modern versus time periods prior to the Quaternary (Shellito & Sloan, 2006a).

https://doi.org/10.5194/egusphere-2026-4262
Preprint. Discussion started: 31 August 2026

Given the well-documented correlations between vegetation distributions and climate but weaknesses in the understanding and data to predict these distributions through state-of-the-art processed-based model simulations, we would like to circle back to original approaches of prescribing climate-derived VBCs and biophysical parameters for GCMs, updating now with data from the satellite era and accumulation of large databases of plant traits. When Matthews (1983, 1984) and Dorman and Sellers (1989) developed their prescriptions of VBCs for the NASA Goddard Institute for Space Studies GCM and the Simple Biosphere Model (SiB) canopy biophysics model, respectively, they relied on literature field data, as this was before the era of the Moderate Resolutions Imaging Spectroradiometer (MODIS) satellites (2001-2026/2027), which were tailored to observing land vegetation attributes globally at high spatial resolution (500 m - 1 km) and multi-day (4-8 days) temporal resolution (Friedl et al., 2002; Myneni et al., 2002; Schaaf et al., 2002). The MODIS data products (cover fraction, LAI, band albedos, and other derived variables) have directly served the DGVM community in identifying distributions of PFTs rather than biomes. An early estimate of global forest heights with lidar data was made from the Geoscience Laser Altimeter System (GLAS) aboard the ICESat (Ice, Cloud, and land Elevation Satellite) at coarse spatial resolutions for the year 2005 (Simard et al., 2011). Emerging data from ICESat-2 (Feng et al., 2023; Neuenschwander et al., 2020; Neuenschwander & Pitts, 2019; Neuenschwander et al., 2019) and the Global Ecosystem Dynamics Investigation (GEDI) (Ralph O. Dubayah et al., 2022; Dubayah et al., 2021) promise together to provide global scale more accurate high spatial resolution estimation of canopy height metrics (Favrichon et al., 2025) as well as provide vertical foliage profiles. These data can be used to quantify biome attributes with regard to their mix of PFTs and their canopy structure, accounting for their geographic variation, and figuring out how to utilize this data in models is the current cutting edge.

Wladimir Köppen (1846-1940) was a geographer who began mapping the correlations between climate, as characterized by temperature and precipitation, and vegetation biomes in the 19th century (Köppen, 1984), developing a detailed classification scheme of over 30 biome types known now as the Köppen-Geiger climate classification scheme (Köppen & Geiger, 1936). This scheme is not perfect, and a later well-known refinement by (Trewartha, 1968; Trewartha & Horn, 1980; Valjarević et al., 2022) was made to better capture the mid-latitudes. Despite other variations on these schemes, the Köppen-Geiger system has remained a reliable and popular framework for interpreting Earth's modern climate record (Kottek et al., 2006; Peel et al., 2007) and for evaluating simulated climates in Earth general circulation models, both for assessing their accuracy as well as projecting potential vegetation shifts with climate change (Beck et al., 2018; Ito et al., 2020; Rubel & Kottek, 2010; Willmes et al., 2017). Poulter et al. (2011) investigated use of the Köppen-Geiger scheme to attribute physiognomy and phenology to climate zone and to assess uncertainty in identification of "plant functional types" (PFTs) in satellite observations; they found the greatest uncertainty in distinguishing cropland and grassland, and shrubland versus forest. For deep-time paleoclimate, Zhang et al. (2016) developed a simplified version of the Köppen-Geiger scheme to utilize the limited climate data from fossil reconstructions of paleoclimate (Burgener et al., 2023; Pohl et al., 2022; Yoo & Rohli, 2016).

We present here a tool for generating VBCs for simulating vegetation biophysics for climate model investigations of the past and future outside the satellite era when the science question does not require full biogeochemical and biogeographical dynamics. In lieu of simulating fully prognostic phenology, growth, and ecological processes to predict seasonal LAI and

https://doi.org/10.5194/egusphere-2026-4262
Preprint. Discussion started: 31 August 2026

cover distributions under different climates, our tool generates Köppen-Geiger climate-biome classification of monthly climatology of surface temperature and precipitation. The tool uses this information to generate a lookup table (LUT) of vegetation boundary conditions by biome class of satellite-derived VBCs of plant functional type subgrid cover fraction, monthly leaf area index, and canopy height, suitable for prescribing in global vegetation biophysics models. We rely on the assumption that the vegetation functional properties of a biome are largely conserved in space given its climate features, particularly with regard to physical attributes of canopy height and leaf area index. This lookup table can then be used to generate VBCs for alternative climatologies. For changes by evolutionary time, for paleo-vegetation in the Phanerozoic Eon from the Cretaceous Period and later, we implemented additional algorithms to remove or replace modern vegetation types with the relevant PFTs according to time period, such as the substitution of C4 grasses by C3 grasses or bare soil prior to their first appearance in the fossil record. To evaluate the efficacy of the LUT, we compared climatological simulations over 1980-2020 with an Earth System Model (ESM) given the original satellite-derived boundary conditions vs. LUT-derived boundary conditions. We also used a GCM simulation configured for the Cretaceous Thermal Maximum at 85 Mya to predict VBCs, comparing to a fossil reconstruction. Finally, we discuss the utility of our LUT tool for generating DGVM vegetation boundary conditions for coupling with climate models.

2 Methods

Observational mean monthly climatologies were used to generate Köppen-Geiger biome type maps. These were used as a mask to tabulate within each biome the statistics of vegetation boundary conditions (VBCs) for 12 plant functional types (PFTs) of the Ent Terrestrial Biosphere Model generated from satellite-derived observations of: subgrid cover fractions, canopy heights, monthly leaf area index (LAI), ,and maximum annual LAI. A lookup table was then constructed tabulating the subgrid cover of PFTs and their canopy boundary conditions for each Köppen-Geiger class. We implemented additional algorithms to modify the modern cover types for late Phanerozoic paleo-vegetation given years before present. The lookup table was then used to regenerate modern VBCs for comparison to the satellite-derived VBCs. To evaluate the efficacy of the LUT-derived VBCs, we compared climatology simulated in a GCM and diagnostics of carbon stocks and fluxes, given the original versus the lookup table-derived VBCs. The lookup table and paleo-vegetation algorithms were also applied to preliminary GCM simulations of Cretaceous climatology to generate a maps of Köppen-Geiger biome classes and Ent cover for comparison to a fossil reconstruction by Saward (1992).

2.1 Köppen-Geiger climate classification

We used the algorithms for Köppen-Geiger (hereafter sometimes abbreviated as "KG") climate classification from Kottek et al. (2006), which produces 31 climate classes, listed in Appendix Table A 1. In addition, we introduce a slight modification for the tropics. Instead of a half-year summer as used by Kottek et a. (2006), we used 4-month seasons for

https://doi.org/10.5194/egusphere-2026-4262
Preprint. Discussion started: 31 August 2026

tropical climates As and Aw (northern hemisphere, summer = June-September, winter = November-February). This identifies the rain shadow areas in East Africa, Sri Lanka, but with slight excess of these types over northeastern Brazil.

2.2 Ent Global Vegetation Structure Data Set

The NASA Goddard Institute for Space Studies (GISS) Earth System Model, ModelE-2.1 uses the Ent Terrestrial Biosphere Model (Kim et al. 2015) as its coupled DGVM. Ent is a demographic DGVM following the approach introduced by the Ecosystem Demography (ED) model of Moorcroft et al. (2001) to represent heterogeneous landscape structure through height-stratified canopies in subgrid landscape patches. Vegetation communities consist of mixes of "cohorts" that are ensembles of identical individual plants, with cohorts distinguished by height and plant functional type. In ModelE-2.1, Ent is run in biophysics-only mode to provide land surface albedo and to simulate exchanges of water vapor and carbon dioxide with the atmosphere. In this mode, canopy structure is prescribed from vegetation boundary conditions (VBCs) from the Ent Global Vegetation Structure Dataset (Ent GVSD) v1.0 (Ito et al., 2020; Kiang et al., in prep.).

The Ent GVSD v1.0 provides mosaicked subgrid fractional cover of 12 Ent TBM plant functional types (PFTs) derived from the Moderate Resolution Imaging Spectroradiometer (MODIS) land cover and PFT products (Friedl et al., 2002; Friedl et al., 2010), annual maximum and monthly leaf area index (LAI) (Tian et al., 2002a, 2002b), and forest canopy heights derived from ICESat/GLAS by Simard et al. (2011); monthly observed MODIS LAI is from the year 2004. C3 and C4 grasses and were further distinguished with climate data from the Princeton Global Meteorological Forcings (PGMF) (Sheffield et al., 2006). These data describe VBCs of 12 Ent PFTs: evergreen broadleaf trees, evergreen needleleaf trees, cold deciduous broadleaf trees, drought deciduous broadleaf trees, deciduous needleleaf trees, cold-adapted shrubs, arid-adapted shrubs, C3 perennial grass, C3 annual grass, C3 arctic grass, C4 grass, and herb crops (with physics of C3 perennial grass). In addition, as a legacy of how land surface albedo was originally specified in ModelE, bare soil cover has a grey albedo (shortwave band 300-4000 nm) and is represented in two fractions of bright soil (albedo 0.5) and dark soil (albedo 0.0). The PFT, height, and maximum annual LAI are used with Ent's allometry functions to estimate vegetation demography (number density of plants) online in single-cohort canopies. We note that the boundary conditions are not specific to demographic DGVMs, and Ent's PFTs are common among DGVMs. The generated cover fractions and seasonal LAI are necessary VBCs that can be used in the vegetation biophysics of other land surface models, and height is additionally necessary for many models. The steps to format the VBCs for input to ModelE are given in the Appendix, Section A.1.

2.3 Ent-Köppen-Geiger VBC lookup table

A lookup table of the Ent PFT and bare soil cover fractions, height, monthly LAI, and maximum annual LAI for each of the Ent cover types in each Köppen-Geiger biome class (Table A 1) was generated through the following steps. For compatible climate data with the Ent GVSD v1.0, which is based on 2004 LAI and 2005 forest heights, we used a contemporary 2001-2010 climatology of mean monthly surface temperature from the Climate Research Unit (CRU TS 3.22) (Harris, 2014; Harris et al., 2014), and the same decade mean monthly precipitation from the Global Precipitation Climatology Centre (GPCC

https://doi.org/10.5194/egusphere-2026-4262
Preprint. Discussion started: 31 August 2026

v6) (Schneider et al., 2011). We note that a coarser resolution climatology at 2.5° x 2.0° is insufficient to capture the less common Dsd biome type, hence the climatology data at 0.5° x 0.5° was classified into a KG biome map. biome classification at 0.5° x 0.5°. Each biome was applied as a mask over the "extended" version of the Ent GVSD v1.0 VBCs to tabulate their statistics in each biome.

For the cover fractions of a biome, we calculated the mean and standard deviations of the masked cover fractions using the grid cell area as the weight, excluded small fractions with a threshold <0.08 (a setting that can be modified in the configuration file), and then rescaled all cover fractions such that the sum is 1.0 for that biome. Because quantities like the canopy height or LAI were not normally distributed, instead of taking the mean and standard deviation, we performed a kernel density estimation (KDE) (Parzen, 1962; Rosenblatt, 1956) over the subset of the data using the PFT cover fraction multiplied by the surface area of each grid cell as the weight. We used Python version 3.12 with packages NumPy and SciPy, function scipy.stats.gaussian_kde, based on Scott (1979), with bandwidth using Scott's Rule for unequally weighted data. The value for the lookup table was generated by choosing the highest peak of the resulting probability distribution, using the function scipy.signal.find_peaks with the standard deviation set as the full width at half maximum of the peak to quantify the spread. Only if there were fewer than 10 grid cells in the resulting set of masked VBC, we used the area-weighted mean and standard deviation. For monthly LAI we calculated the KDE statistics separately by 6 months for the northern and southern hemispheres (NH and SH) for each biome to account for opposite seasonality. These hemisphere peak values were then averaged together using the sum of weights of each hemisphere, and accounting for the inverse seasonality of the hemispheres, to produce a final monthly LAI curve for that PFT and biome. However, for equatorial biome Af, we did not distinguish opposing seasonality across the equator, but we just combined all grid cells in that biome and took the global average for the observed monthly values. For maximum LAI, instead of using the source maximum LAI, we assigned the maximum monthly LAI from the KDE statistics as the maximum for that PFT and biome. to calculate weighted means of height, LAI, and maximum annual LAI. For biomes where few grid cells exist, we used just the one grid cell in lieu of a regression. This was done for Csc and Cwc biomes. For biomes that exist only in one hemisphere, the monthly LAI data was mirrored for the other hemisphere, with the data shifted by six months to preserve seasonality.

To ensure the lookup table accounts for the possibility that it might be applied to a climatology that has climate classes unrecognized by the Köppen-Geiger classification system, we formulated default bare soil albedo assignments for undefined climate types, which we gave class labels starting with "U". To these "U" classes we assigned cover fractions as follows: for undefined equatorial climates (UA, UAu), 0.3 bright soil and 0.7 dark soil, which gives a grey albedo 0.15; for arid climates (UB), 0.6 bright, 0.4 dark, given an albedo of 0.3, based on an average for the BWk and BWh; for polar and snow climates (UE, Ufu), 0.82 bright, 0.18 dark, giving an albedo of 0.41, based on the values for the EF biome; and where there is no clear climate category (Uuu), the defaults are the values for arid climates. Of these "U" climates, actually only Ufu can possibly be generated, whereas others are error catching categories in case of incorrect use of the classifying algorithms. These steps generated the final lookup table (referred to hereafter as "EntKGLUT"); the frozen version of the EntKGLUT is provided in the Table A 2 in the Appendix, and as a netcdf file in the Supplementary Material.

https://doi.org/10.5194/egusphere-2026-4262
Preprint. Discussion started: 31 August 2026

Albedo is a major feature of vegetation that impacts climate (Charney et al., 1975). Our LUT does not generate albedos, because ESM-coupled global vegetation models have internal canopy albedo schemes, which depend on their canopy radiative transfer (CRT) approach. In the coupling of Ent to ModelE, the seasonal vegetation albedos are generated from a lookup table by PFT, that is a translation of the albedos by biome types developed by Matthews (1984) from literature measurements (Schmidt et al., 2006). This scheme is Lambertian and not sensitive to geographically varying LAI for a PFT. Other models may have prognostic albedo assuming CRT with plane-parallel homogeneous canopy structure and end member optical properties in two-stream schemes, while a few models have approaches to account for canopy gaps (Fisher et al., 2018; Haverd et al., 2012; Ni-Meister et al., 2010). Advancing how vegetation models predict albedo is an area of continuing research (Widlowski et al., 2015; Widlowski et al., 2011; Widlowski et al., 2013). For this study, we relied on the ModelE-Ent internal surface albedo algorithms.

2.4 GCM vegetation boundary conditions files

Given the lookup table generated as described in Section 2.3, one generates the VBCs for a particular global climatology by supplying the climatological mean monthly surface temperature and precipitation to generate its Köpper-Geiger biome map, and then applying the lookup table to that biome map. NetCDF files for any climatology of monthly surface temperature and precipitation can be used to generate boundary conditions from equilibrated runs for different climatologies, such as for pre-industrial climate and paleoclimates. We supply a script that performs these steps and returns netCDF file maps of the corresponding boundary conditions for PFT cover fractions, canopy height, monthly LAI, and maximum LAI. These netCDF files are formatted for input directly to the NASA GISS ModelE-2.1. A wrapper script is also available to process directly simulated climatological diagnostic outputs from ModelE for convenient input to the Köppen-Geiger utility.

2.5 Paleovegetation

The EntKGLUT is based on modern vegetation, so modifications are needed to generate paleo-vegetation boundary conditions. Since some of modern plant functional types had not yet evolved in some earlier time periods, we implemented additional optional steps for post-processing the modern vegetation boundary conditions to replace anachronistic types with the most closely relevant cover type for paleoclimates. The replacements are valid going back to the latest Jurassic/start of the Cretaceous. Prior to this the Ent PFTs do not fully represent some earlier plant types that would have been dominant, and use of our tool is not recommended.

https://doi.org/10.5194/egusphere-2026-4262
Preprint. Discussion started: 31 August 2026

Table 1. Late Phanerozoic Eon periods and time ranges for emergence and spread for specific plant functional types. Time ranges of the geological period are from the International Commission on Stratigraphy (https://stratigraphy.org/chart/). Emergence times are estimated from the literature (see text). Colors are from the RGB color codes of the Commission of the Geological Map of the World (CGMW), Paris, France.

Period	Period time range (Mya)	Emergence times (Mya)	Plant functional type
Quaternary	2.58 Mya - present		
Neogene	23 to 2.58 Mya		
Paleogene	66 to 23 Mya	32 to 8	C4 grasses emerged
		47.5 to 26	cold-tolerant grasses emerged
		66 to 20	deciduous broadleaf trees emerged
Cretaceous	145 to 66 Mya	80 to 50	C3 grasses emerged
		120 to 80	deciduous needleleaf trees emerged
Jurassic	201.3 to 145 Mya	150	evergreen needleleaf trees existed

2.5.1 C3 and C4 grasses

We took C3 grass and C4 grass evolution timing and spread from Strömberg and McInerney (2011). The earliest fossil evidence of grass-dominated ecosystems is around 80 Mya (Strömberg, 2011), but grasses emerged earlier, very likely in shaded or transition margins between forest understory and open areas (Gallaher et al., 2022). Fossil evidence of silica phytoliths in China has been found as early as 113-101 Mya (Wu et al., 2018), and phylogenetic analysis estimate 98.54 Mya (Gallaher et al., 2022) to 101 Mya (Huang et al., 2022) for the crown age of *Poaceae.* C3 grasses were distributed worldwide by the early Eocene ~56 Mya. The timing of C4 grasses, with multiple independent origins, continues to be studied and debated. We set their date of emergence as 32 Mya, spreading to their modern levels of competitiveness by 3-8 Mya (Edwards et al., 2010; Sage, 2001; Strömberg & McInerney, 2011). Annual grasses emerged later than perennials, but it is not well-known when; therefore, we retain both perennial and annual C3 grass types if they exist in the modern classification. Cold tolerance in arctic C3 grasses also likely emerged not till 47.5 Mya reaching mature distributions by 26 Mya (Preston & Sandve, 2013). Therefore, we specified a decision tree for grass emergence as follows:

1. If the paleoclimate is before 80 Mya, then all grasses are replaced with bare soil.

2. If within 80-50 Mya, then perennial and annual C3 grasses are ramped up linearly from a fraction of 0% of its modern KGLUT predicted value at 80 Mya to 100% at 50 Mya.

3. At 47.5 Mya, arctic C3 grasses emerged, and their fraction of their modern-predicted cover fractions is ramped up linearly to their total modern-predicted cover fraction by 26 Mya.

4. At 32 Mya, C4 grasses emerged, and their fraction of their modern-predicted cover fractions is ramped up linearly from a fraction of 0% of its modern-predicted value at 32 Mya to 100% times its modern-predicted value at 8 Mya. If the modern EntKGLUT predicted any of Ent's three C3 grass PFTs in a grid cell, then their cover fractions are scaled up

https://doi.org/10.5194/egusphere-2026-4262
Preprint. Discussion started: 31 August 2026

proportionately to replace the C4 grass fraction that should not be there; otherwise, if no C3 grasses present, then the C4 grass is replaced with C3 perennial grass proportionately to its temporal relative dominance.

2.5.2 Deciduous broadleaf trees

The deciduous habit of broadleaf trees did not evolve before ~66 Mya at the K/Pg boundary, and then after they emerged, their spread reached maturity in the Miocene around 20 Mya (Crane & Lidgard, 1989; Vajda & Bercovici, 2014). This is now known to be regulated by distinct genes responsive to temperature versus photoperiod cues, with not all deciduous species capable of both (Moon et al., 2022; Wilczek et al., 2010). The Ent PFTs currently are not partitioned into distinct types for these genetic types, and the deciduous broadleaf tree PFT encompasses both sensitivities. The modern trees occur in temperate climates, and toward higher latitudes they compete and mix with evergreen needleleaf trees, with a temperate/boreal transition to evergreen needleleaf forest. Therefore, our paleovegetation post-processing rules are:

1. If before 66 Mya, replace Ent PFTs cold deciduous broadleaf and drought deciduous broadleaf with evergreen needleleaf.
2. From 66 Mya to 20 Mya, ramp up dominance of deciduous broadleaf trees (Ent PFTs cold deciduous broadleaf and drought deciduous broadleaf) from 0% of their KGLUT predicted cover at < 66 Mya to 100% of their KGLUT predicted cover at 20 Mya, scaling up other existing PFTs to replace the fraction cover of deciduous broadleaf trees.

2.5.3 Deciduous needleleaf

Deciduous needleleaf trees (*Larix*, larch; *Metasequoia*, dawn redwood; *Pseudolarix*, golden larch; *Taxodium*, bald cypress; and *Glyptostrobus*) did not evolve until ~120 Mya (Herman & Sokolova, 2016; LePage & Basinger, 1995; Rothwell et al., 2020; Tang et al., 2019), then spread slowly to modern levels of dominance by 80 Mya (Liu et al., 2007). In the Cretaceous, deciduous needleleaf forests were co-dominated by *Glyptostrobus* and *Metasequoia* (Tang et al., 2019), and were replaced by larches in the Paleogene (LePage & Basinger, 1995; Liu et al., 2007). Therefore, our paleo-vegetation post-processing rules for deciduous needleleaf trees are:

1. If before 120 Mya, then replace Ent PFT deciduous needleleaf with evergreen needleleaf.
2. From 120 Mya to 80 Mya, ramp up dominance of deciduous needleleaf from 0% of its KGLUT predicted cover fraction to 100%, with the replaced fraction changed to deciduous needleleaf.

2.5.4 Paleo-vegetation LAI and height

To provide LAI and height values for paleo-vegetation cover types that replace other cover, we adopt the following algorithms, which basically retain the original LAI and height that were there, keeping it for the PFT that was otherwise removed, and assigning it to the replacing PFT. If bare soil replaces a PFT, then bare soil is kept bare, of course. To make this clear why:

https://doi.org/10.5194/egusphere-2026-4262
Preprint. Discussion started: 31 August 2026

1. If the PFT already existed in the grid cell and its cover is merely expanded, then its existing subgrid patch LAI and height are retained.
2. If the PFT did not previously exist in the grid cell, the same growth form is assigned the values of the same growth form it replaces (e.g. grass LAI of previous PFT is kept for the replacing grass type; tree LAI of previous PFT is kept for the replacing tree type).
3. There are no cases of replacing one growth form with a different growth form.
4. If bare soil replaces a PFT, the replaced PFT's LAI and height are still retained in the VBC files. Their values can be scaled by the cover fractions during climate simulations, which will be zero if the PFT is not present. Bare soil simply remains with zero LAI and height.

2.6 Modern Earth ModelE experiments

To evaluate the efficacy of biome statistical VBCs for simulating climate, we used the EntKGLUT derived from the 0.5° x 0.5° climatology to reproduce the Modern 2001-2009 VBCs at 2.5° x 2° using the same climate data regridded at 2.5° x 2° for input to the NASA GISS Earth System Model (ESM) ModelE2.1 (Kelley et al., 2020) (code checkout date April 3, 2018). This ESM has a horizontal grid at 2.5° x 2° and 40-layer atmosphere. ModelE2.-1 was used to simulate modern climatology over 2000-2009, comparing the simulated climatology with the original satellite-derived VBCs to that with the simplified LUT-derived KG biome-specified VBCs.

We conducted two simulations with non-interactive chemistry ("NINT"). Both simulations consisted of a preindustrial spin-up to equilibrate soil carbon at 1850 conditions following the protocol described in Ito et al. (2020). Sea surface temperatures (SSTs) and sea ice cover and thickness were from Hurrell et al. (2008); historical annual average CO_2 mixing ratios 1850-2020 from the 2021 version of forcings from Sitch et al. (2024); historical annual average N_2O, CH_4, and other gases as described in Miller et al. (2021) for 1850-2014, and Lan et al. (2022) for 2015-2020. The 1850 spinup and a short transient period 1850-1870 used a preindustrial climatological 1876-1885 average, and 1870-2020 use annual SSTs and sea ice cover but the climatological average sea ice thickness. The experiment, "E0" used the standard ModelE vegetation boundary conditions from the Ent GVSD. The second experiment, "E1", used the EntKGLUT-generated vegetation boundary conditions. All other input files and parameters were identical between the two runs. The Ent model in each experiment was spun up using pre-industrial conditions (1850), first by running for 30 years to spin up plant labile carbon, and secondly running 9 years to collect climate forcings which are repeated for 6750 years to spin up soil carbon. The spinups were conducted 3 times for each experiment. Then, the runs proceeded using transient conditions from 1850 to 2020. We then analyzed climatology over 2000-2009, which is the decade in which our satellite VBCs were derived.

https://doi.org/10.5194/egusphere-2026-4262
Preprint. Discussion started: 31 August 2026

2.7 Cretaceous preliminary paleo-vegetation boundary conditions

For evaluation of prediction of paleo-vegetation boundary conditions at the Cretaceous at 85 Mya, we conducted two preliminary steps for asynchronous equilibration of climate and vegetation. We used the Resolving Orbital and Climate Keys for Earth and Extraterrestrial Environments with Dynamics version 2.0 planetary climate model (ROCKE-3D, planet 2.0) (Tsigaridis et al., 2025; Way et al., 2017). The model simulates a fully dynamic ocean with "bathtub" bathymetry (Tsigaridis et al., 2025) and 1300 m maximum m depth. The experimental configuration used a 4°x5° horizontal grid and 40-layer atmosphere. Continental boundary conditions were derived from the 1°x1° paleo-digital elevation models (paleoDEMs) version 1 by Scotese and Wright (2018) and down-sampled to the ROCKE-3D resolution. Hand adjustments were made to remove isolated ocean grid cells and connect oceans with open channels. A modern solar spectrum was used, but with the solar constant reduced to 1350.58 W/m^2, modern obliquity, a rotation period of 85,176 s appropriate for the Cretaceous (Waltham, 2015), CO_2 mixing ratio of 1500 ppm, 2 ppm CH_4, and a global mean surface pressure of 1136 mb. For initial conditions for surface cover, continents were specified with bare soil with soil texture as all sand. Albedo of soil was uniformly 0.2384, from prescribing 47.68% bright soil (albedo 0.5) and 52.32% dark soil (albedo 0.0). The model was spun up to hydrological and climatological equilibrium over 1500 years, and the last 10 years of the simulation were used for the average climatology. The surface cover was then asynchronously updated using the EntKGLUT and paleo-vegetation cover algorithms to derive VBCs from the bare soil climatology. These VBCs were then prescribed, and the simulation was restarted and re-equilibrated, and the last 10 years' average climatology used for second EntKGLUT classification. We then compared the climate and vegetation cover changes between these two iterations.

3 Results

3.1 Köppen-Geiger Ent modern boundary condition maps

Figure 1a shows the Köppen-Geiger biomes from classifying the observed 2001-2009 climatology at 0.5° x 0.5° for the EntKGLUT. Figure 1b, c, d, and e show, respectively, the satellite-derived Ent TBM cover types (dominant type per grid cell shown), the dominant natural vegetation cover from scaling out crop cover, and the cover-weighted cell average canopy heights and maximum annual LAI. A table of the Ent subgrid natural cover fractions for each biome is shown in the Appendix in Table A 1. The Supplementary Material further provides, for handy reference, a spreadsheet file of tables of natural cover fractions, heights, and maximum LAI, and a netCDF file of the full EntKGLUT including monthly LAI.

https://doi.org/10.5194/egusphere-2026-4262
Preprint. Discussion started: 31 August 2026

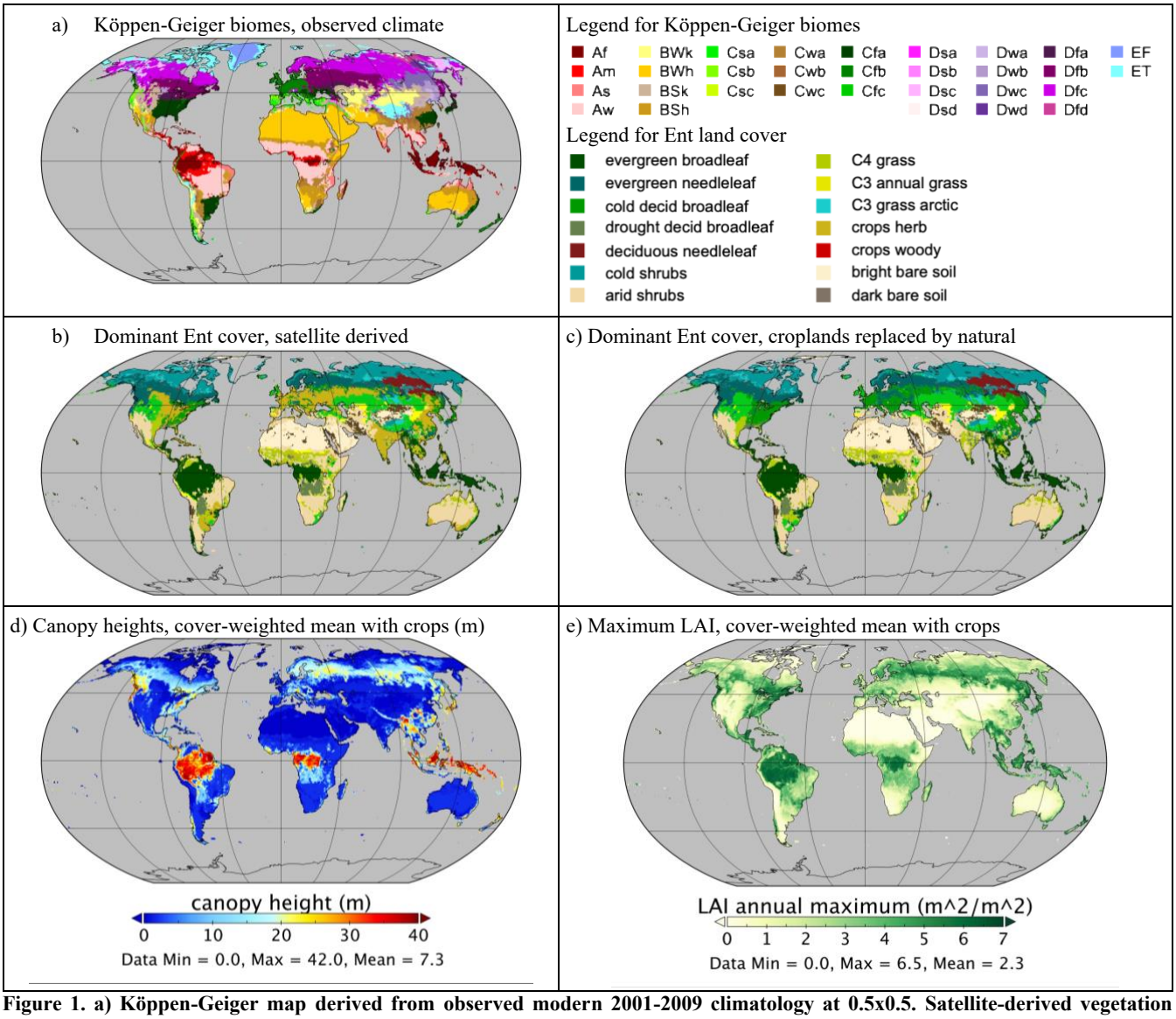

Figure 1. a) Köppen-Geiger map derived from observed modern 2001-2009 climatology at 0.5x0.5. Satellite-derived vegetation boundary conditions data from the Ent Global Vegetation Structure Dataset v1.0, showing b) dominant Ent cover types derived from satellite data, c) dominant Ent cover types from with croplands replaced with local natural vegetation, d) cover-weighted canopy heights with crops, and e) cover-weighted maximum annual LAI with crops. Monthly LAI and details by cover type may be viewed in the Supplementary Material.

3.2 Distributions of VBCs by biome and cover type

The KDE algorithm successfully identified the peaks in the frequencies of height and LAI by biome and cover type. The full details of all distributions and their fitted KDE values are plotted in the Supplementary Material. In Figure 2 we show an example of the Af biome. This tropical biome is dominated by evergreen broadleaf trees while other cover types have very low cover, such that the LUT assigns this biome 100% evergreen broadleaf trees with a mean maximum LAI of 5.55.

https://doi.org/10.5194/egusphere-2026-4262
Preprint. Discussion started: 31 August 2026

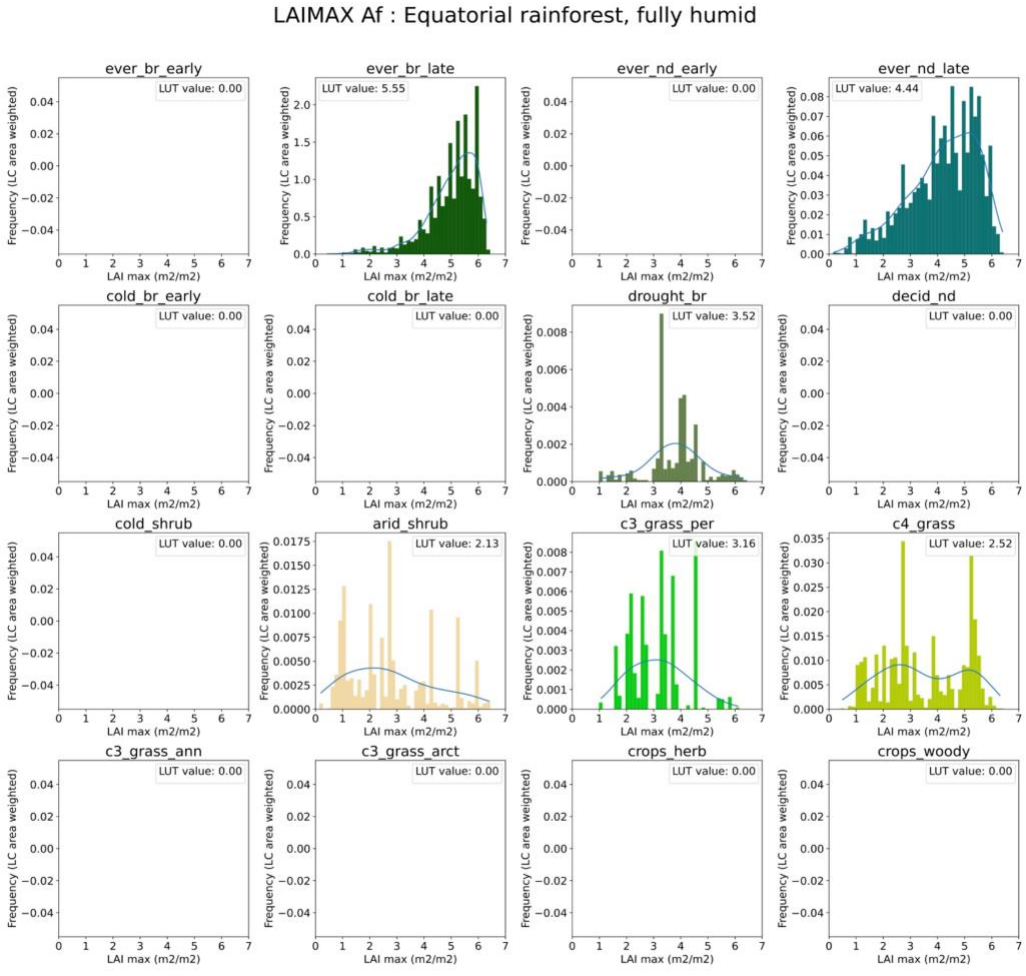

Figure 2. Distribution of maximum annual LAI by cover type for the Af biome ("Equatorial rain forest, fully humid"), showing the KDE fitted curves and selected lookup table (LUT) values at the peak.

3.3 Regenerated Modern Vegetation Boundary Conditions from the LUT

Figure 3 shows the biome distributions and natural vegetation-only VBCs regenerated from the EntKGLUT for observed 2001-2010 climatology at 2.5° x 2°. Figure 3b, c, d show the dominant cover, canopy height, and maximum annual LAI of Ent PFTs for natural with croplands scaled out and replaced by the natural PFTs in that grid cell (the subgrid fractions of the PFTs are available in the Supplementary Material). Figure 3e, f, g, have cropland cover scaled back in. Without cropland, the cover-weighted mean canopy heights are taller and the mean maximum annual LAI larger than the original data, while the maximum for both is lower than in the original data.

https://doi.org/10.5194/egusphere-2026-4262
Preprint. Discussion started: 31 August 2026

a) 2.5° x 2° Köppen-Geiger classification

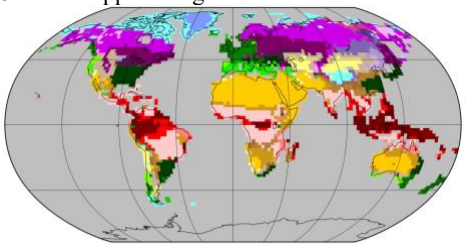

b) Dominant Ent cover types, natural vegetation only

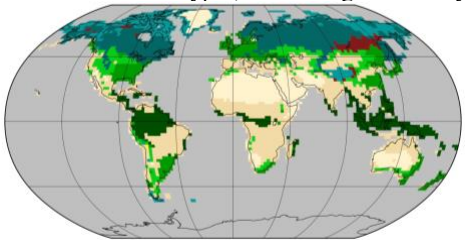

c) Dominant Ent cover types, with 2004 observed crop cover

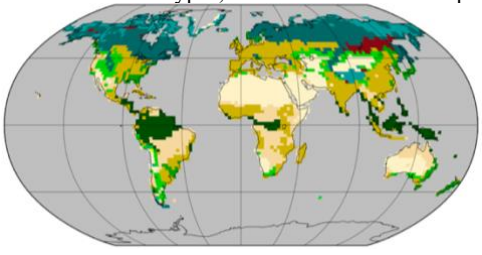

d) Canopy heights, natural vegetation-only

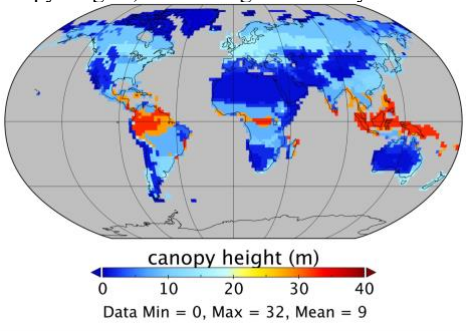

e) Canopy heights, with 2004 observed crop cover

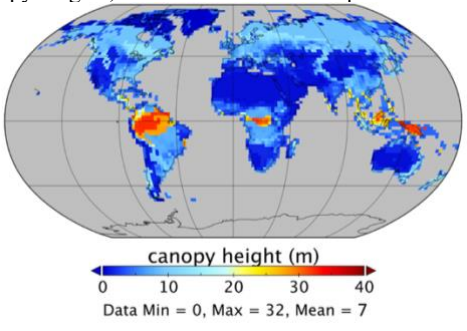

f) Maximum annual LAI, natural vegetation-only

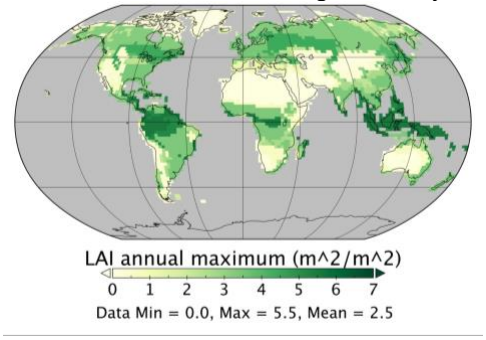

g) Maximum annual LAI, with 2004 observed crop cover

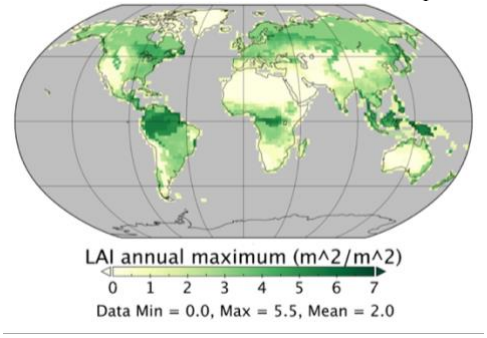

Figure 3. a) Köppen-Geiger biomes for the same climatology as Figure 1 but at 2.5° x 2°. b) EntKGLUT-derived natural vegetation cover (without crops). Grid cover-weighted averages for natural vegetation only for: d) canopy heights, e) maximum annual LAI. VBC's with 2004 crop cover: c) dominant Ent land cover, g) canopy height, g) maximum annual LAI . Legends for Köppen-Geiger classes and Ent land cover types are as in Figure 1. Monthly LAI and details by cover type may be viewed in the Supplementary Material.

An averaged climatology at 2.5° x 2° is too coarse to capture a less common climate type, Dsd, while the 0.5° x 0.5° grid scale is precise enough to identify this climate type. Because the VBC distributions generated from the LUT are statistical properties of the biome types wherever they occur, and because we combined the statistics for each biome type from both

https://doi.org/10.5194/egusphere-2026-4262
Preprint. Discussion started: 31 August 2026

hemispheres, the Cfb and Cfc biomes exhibit some cover of broadleaf evergreen trees where they do not normally in the NH, because these biome types in the SH do have broadleaf evergreen trees. Similarly, evergreen needeleaf trees, which are less prevalent in the SH, have increased average cover in the reproduced VBCs. Because the Köppen-Geiger boreal climate class Df (magenta color) (Figure 1a) covers both evergreen needleleaf boreal forest (dark blue-green) and tundra (medium blue-green) (Figure 1b), the averaging of their cover fractions leads to broader distributions of both across the Df biome than observed, with evergreen needleleaf trees dominating (Figure SM1, 3rd column). The semi-arid climate type Aw (pink) covers savannahs with varying tree/grass ratios that range from dominance by C4 grassland (yellow-green) in northern Africa, drought deciduous trees (dark grey-green) south of the Congo Basin, and arid shrubland in eastern Brazil, resulting in shrubland dominating the biome class. Similarly for the hot arid climate BWh (dark yellow) covering both African and Middle Eastern desert (bright soil, light tan) and Australian shrubland (darker tan), averaging these leads to the biome class being dominated by sparse shrubland.

3.4 Model experiments

3.4.1 Modern climate

Figure 4 shows the ground albedos as estimated by MODIS and in the two ModelE experiments for the Modern. The ground albedos are due to vegetation, soil, soil moisture, and snow/ice. E1 has lower albedo than E0 in the northern high latitudes, because the Köppen-Geiger classification for Dfc extends across boreal forest and northward where forest does not extend in the MODIS observations. Therefore, the EntKGLUT-generated VBCs average across the Dfc region, spreading evergreen needleleaf trees farther north than observed (Figure S1 in the Supplementary Materials provides maps of all subgrid cover fractions). The Köppen-Geiger scheme classifies both the Sahara and the Australia interior as BWh ("Arid desert hot"). The Sahara is mostly bare bright soil while Australia has extensive shrubland. Combining their cover statistics for the EntKGLUT causes the Sahara to be assigned excess arid shrubs and underestimated bare bright soil causing underestimated albedo, with the opposite bias for Australia. These differences, however, are not large enough to alter the simulated climate.

Figure 5 shows observed decadal climatologies for 2000-2009, comparing reanalysis observations of surface air temperature and precipitation from ERA5 (Hersbach et al., 2020) (Figure 5a,d) to experiment E0 (Figure 5b,d) and the difference of experiments of E1-E0 (Figure 5c,f). ModelE-2.1 exhibits a cool bias of -0.6 °C in mean surface temperature for 2000-2009. because we had retained preindustrial sea surface temperatures and sea ice (Figure 5b). E1 with the Köppen-Geiger simplified VBCs has a mean difference from E0 of +0.°C (Figure 5c), primarily warming the high latitudes and poles where the regenerated VBCs have darker albedo, but surprisingly showing little difference in the Sahara and Australia, possibly because these regions are arid climates and sensible heat fluxes dominate. With precipitation, the reproduced VBCs make no difference in the global mean, with regional differences not greater than an absolute 2.7-2.8 mm/day (Figure 5f). We can conclude that the reproduced VBCs are sufficient for simulating modern climates without adversely impacting results, given the uncertainties in VBCs and observed climate.

https://doi.org/10.5194/egusphere-2026-4262
Preprint. Discussion started: 31 August 2026

422

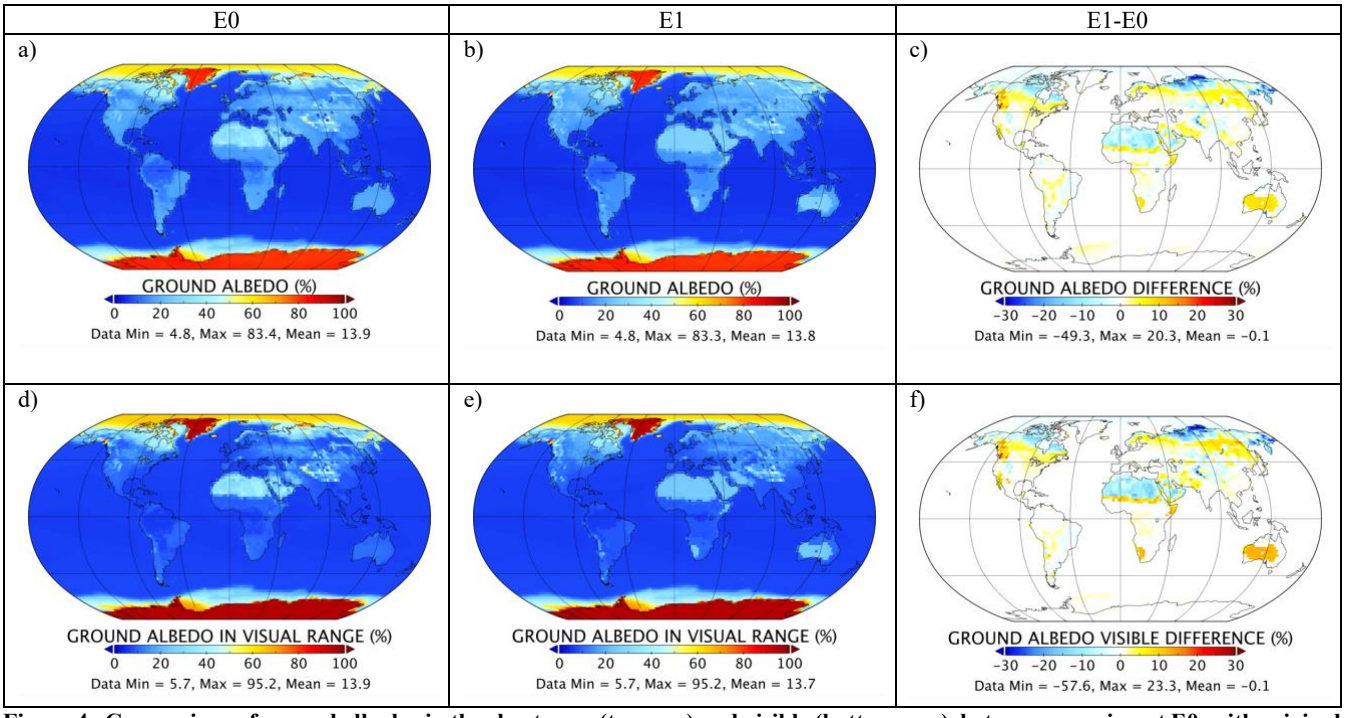

423 **Figure 4. Comparison of ground albedos in the shortwave (top row) and visible (bottom row) between experiment E0, with original**
424 **satellite-derived Ent GVSD v1.0 VBCs (left column, a, d), and E1, with regenerated VBCs with observed climate (middle column, b,**
425 **e), and their difference (right column, c, f).**
426

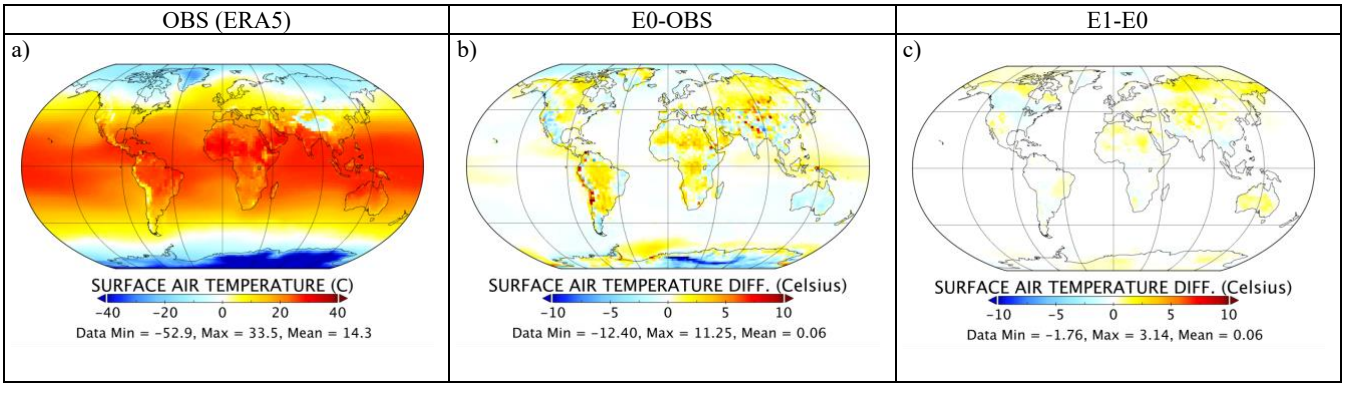

https://doi.org/10.5194/egusphere-2026-4262
Preprint. Discussion started: 31 August 2026

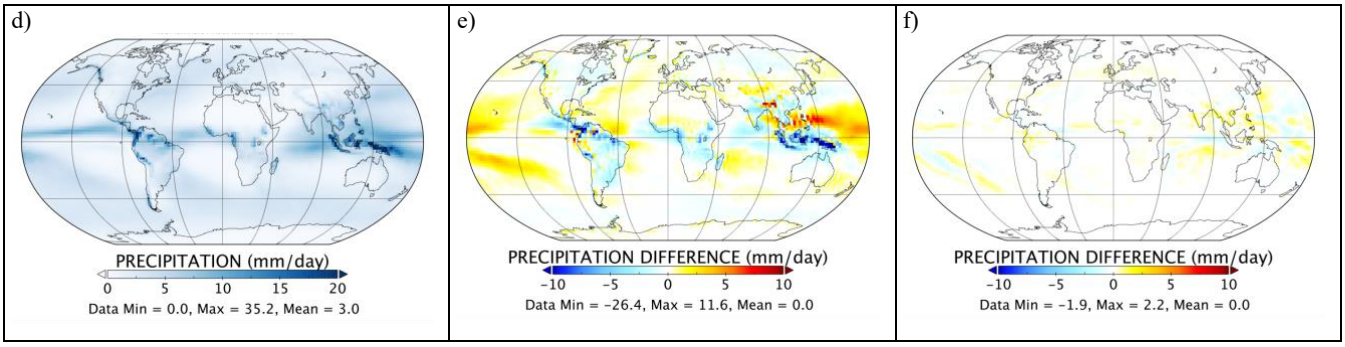

Figure 5. Mean annual surface air temperature and precipitation for decade 2000-2009 comparing: (left column) observations, OBS (ERA5); (middle column) E0-OBS; right column(E1-E0).

Although in these experiments we prescribe atmosphere CO_2 and do not simulate a coupled carbon cycle, it is still useful with this model configuration to examine surface carbon fluxes and stocks estimated by the vegetation model for model evaluation or to compare productivity in different time periods or climates. For our EntKGLUT-generated VBCs, these carbon metrics are also useful for evaluating the efficacy of the LUT for reproducing these biogeochemical quantities. Figure 6 shows global mean annual carbon fluxes (gross primary productivity, GPP; net primary productivity, NPP; net ecosystem exchange, NEE) and soil carbon for experiment E0 with the Ent GVSD v1.0 and the difference of E1-E0. The estimated global mean annual GPP of 122.6 PgC over 2000-2009, is within the range and at the lower end of both multi-model and observation-based estimates ranging 110-170 PgC/yr (Anav et al., 2015; Cheng et al., 2017; Xu & Chen, 2024). The latest Global Carbon Budget 2024 estimates a mean annual GPP of 130 PgC over 2014-2023 (Friedlingstein et al., 2025). The GPP with the EntKGLUT-generated VBCs for experiment E1 is 3.1 PgC/year greater than E0 (Figure 6b). There are regional differences, the largest being an increase of 4.3 kgC/year. The E1-E0 differences in NPP, NEE, and global soil carbon are all well within the range of uncertainties.

Figure 7 shows comparison maps of the model simulated aboveground biomass in experiments E0 and E1 and two observation-based estimates by Spawn et al. (2020) (hereafter referred to as "Spawn2020") and GEDI (R.O. Dubayah et al., 2022). The global total aboveground biomass and differences are given in the plot labels, except for the difference between GEDI-Spawn2020, because the GEDI sensor does not observe above latitude 51.6 °N. Global vegetation biomass estimates are highly uncertain and range 380-536 PgC (Erb et al. 2018). The Spawn2020 estimated total is ~409 PgC. The forest heights in Simard et al. (2011) are now known to be very overestimated by ~6+ m, so their use to assign canopy heights in the Ent GVSD v1.0 results in excess tree stem biomass. There is also a bug in the Ent model in simulation of grasses, in which the carbohydrate reserve pool was scaled incorrectly causing excess grassland biomass. While the Ent with the Ent GVSD v1.0 broadly captures the spatial distribution of biomass carbon density, it overpredicts global aboveground biomass in E0 at 615.7 Pg, outside the range of most estimates. Experiment E1 with the reproduced VBCs results in a global mean increase in biomass, but with regional differences where mean heights and mean maximum annual LAI rectifies some biases or exacerbates others.

https://doi.org/10.5194/egusphere-2026-4262
Preprint. Discussion started: 31 August 2026

The GEDI aboveground biomass product is also biased high in forests compared to Spawn2020, but less extreme than the Ent biases caused by the overestimated forest heights.

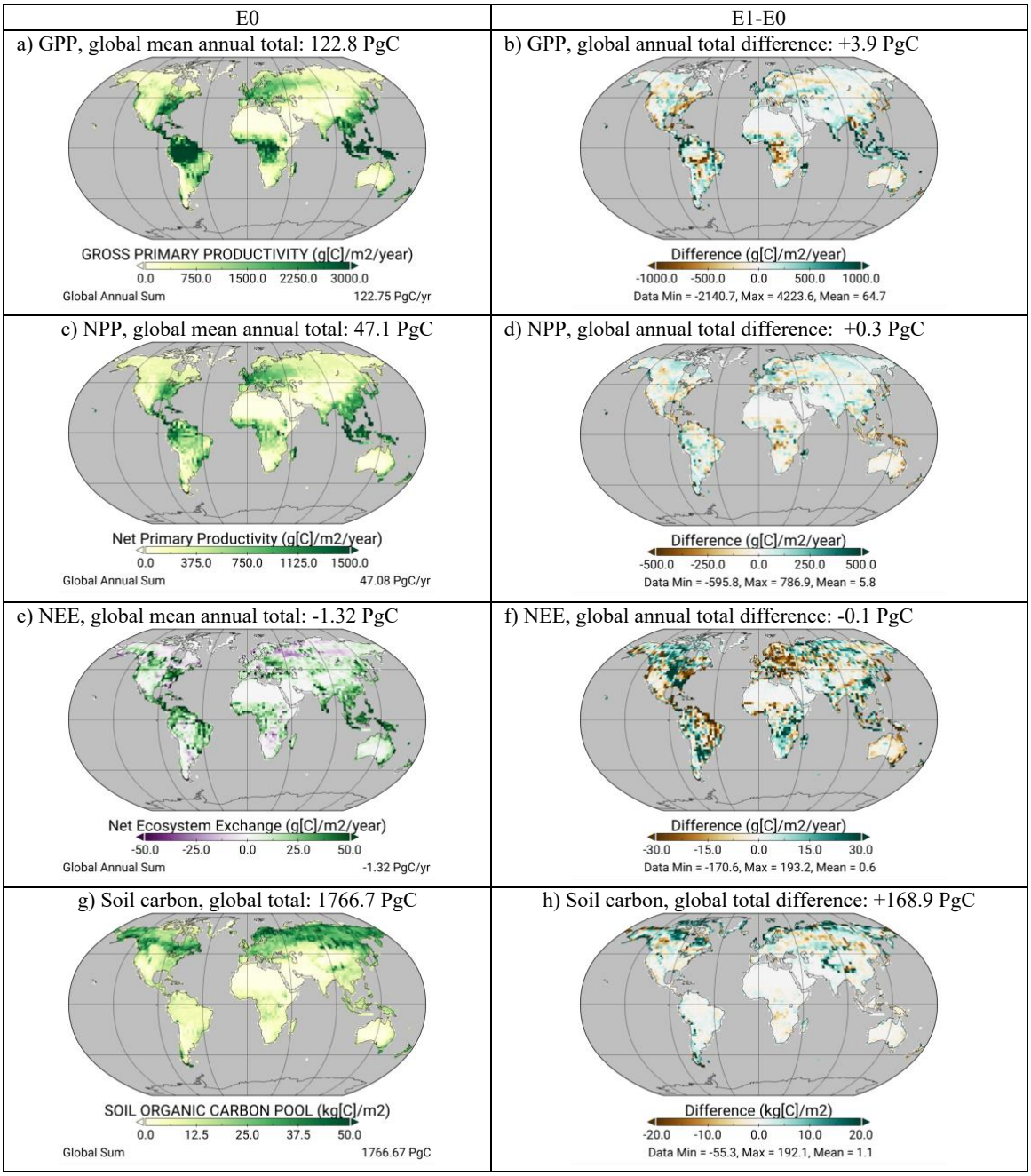

Figure 6. Global mean annual carbon fluxes and soil carbon for 2000-2009 for E0 and difference E1-E0: a-b) GPP, c-d) NPP, e-f) NEE, g-h) soil carbon.

https://doi.org/10.5194/egusphere-2026-4262
Preprint. Discussion started: 31 August 2026

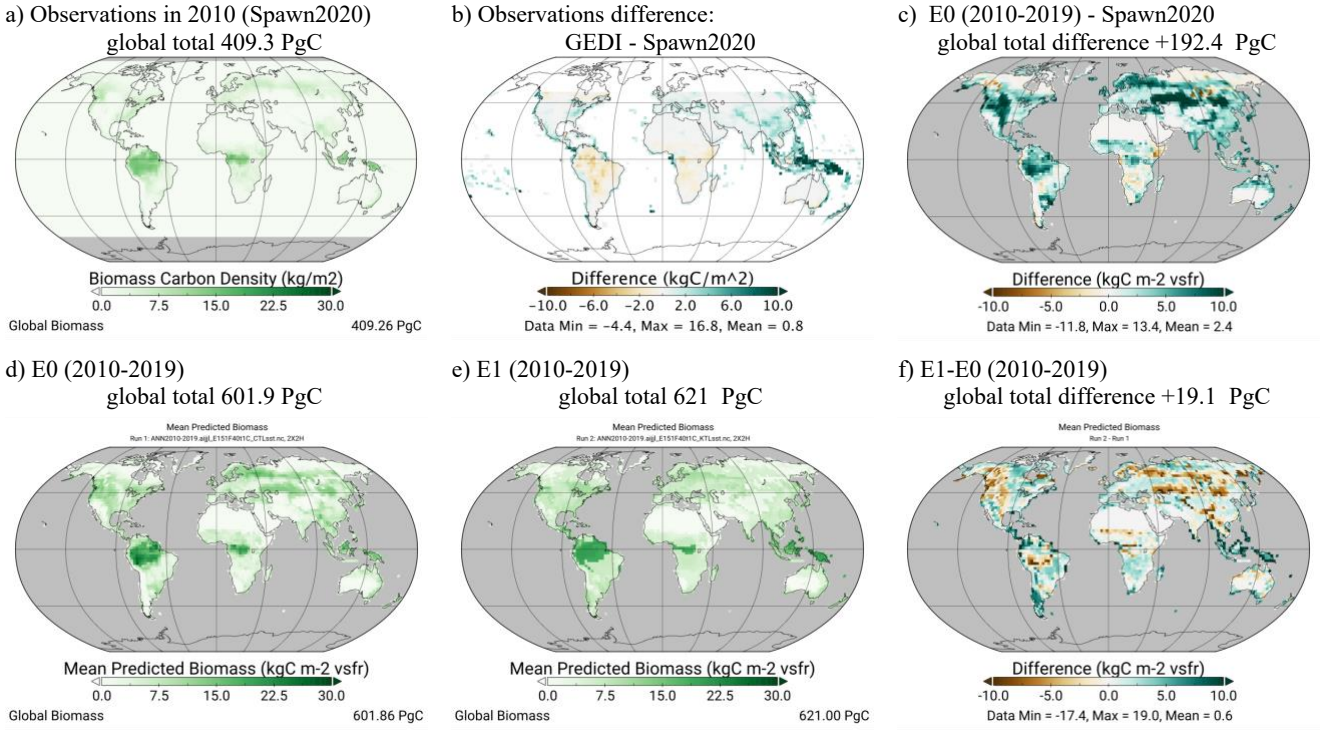

Figure 7. Aboveground biomass: a) observational estimate, Year 2010 (Spawn et al., 2020), "Spawn2020"; b) GEDI - Spawn2020, c) E0-Spawn2020, d) E0 (2010-2019), e) E1(2010-2019), f) E1-E0 (2010-2019).

3.4.2 Cretaceous vegetation asynchronous coupling

The Köppen-Geiger climate classifications, predicted paleo-vegetation VBCs, and climatology diagnostics for our two iterations of bare soil and asynchronously updated vegetation cover for the Cretaceous at 85 Mya at 1500 ppm CO_2 are shown in Figure 8. Figure 8a shows the Köppen-Geiger biome classes for the initial bare soil climatology. The dominant Ent PFT cover distributions generated from the modern vegetation EntGKLUT are shown in Figure 8b, and after replacing the modern vegetation with relevant PFTs for 85 Mya the dominant paleo-vegetation cover types are shown in Figure 8c. Our paleo-vegetation ruled described in Section 2.5 resulted in the following replacements of the modern vegetation types:

1. All grasses were replaced with: 30% bare bright soil, 70% bare dark soil.
2. Drought deciduous broadleaf tree was replaced with evergreen needleleaf tree.
3. Cold deciduous broadleaf tree was replaced with evergreen needleleaf tree.
4. 12.50% of deciduous needleleaf tree was replaced with evergreen needleleaf tree.

Thus, our rules for emergence and spread of different PFTs account for the Cretaceous at 85 Mya lacking grasses and deciduous broadleaf trees, and that deciduous needleleaf trees had not spread to their full level of prevalence. Figure 8d and e show the grid cell cover-weighted average canopy height and maximum annual LAI corresponding to the 85 Mya vegetation

https://doi.org/10.5194/egusphere-2026-4262
Preprint. Discussion started: 31 August 2026

cover of Figure 8c. NetCDF data files providing maps of the Köppen-Geiger classes, subgrid fractions of all cover types, canopy heights, maximum annual LAI, and monthly LAI are provided in the Supplementary Material.

a) Köppen-Geiger climate classes for simulated initial bare soil Cretaceous climatology at 85 Mya.

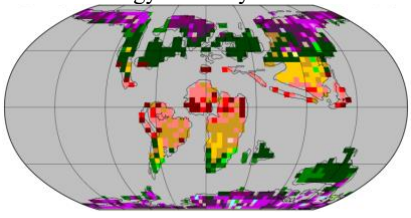

b) Modern dominant Ent cover types for biome classes in a).

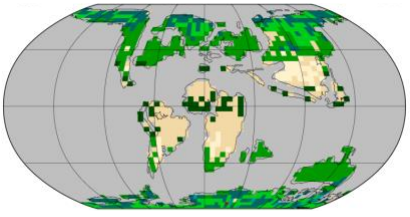

c) Paleo-vegetation dominant Ent cover types for biome classes in a).

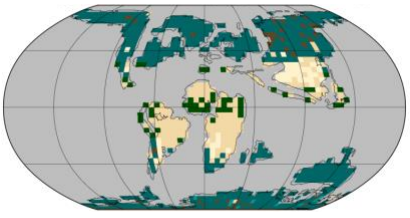

d) Paleo-vegetation canopy heights for 85 Mya

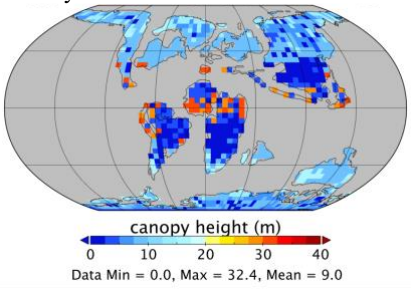

e) Paleo-vegetation maximum annual LAI for 85 Mya

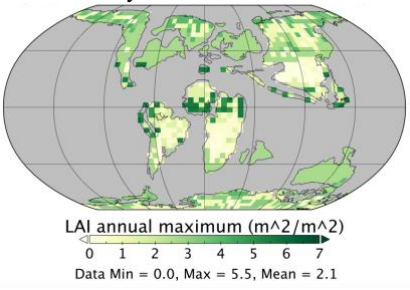

f) Annual mean surface air temperature for bare soil climatology.

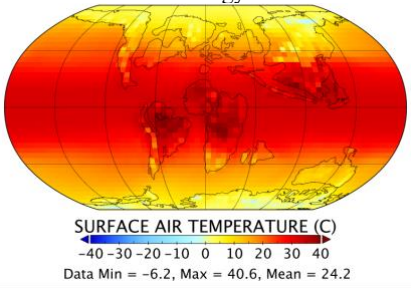

g) Annual mean surface air temperature of climatology with VBCs c, d, e.

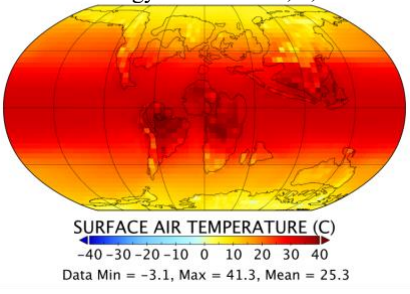

h) Annual mean surface air temperature difference of g) minus f).

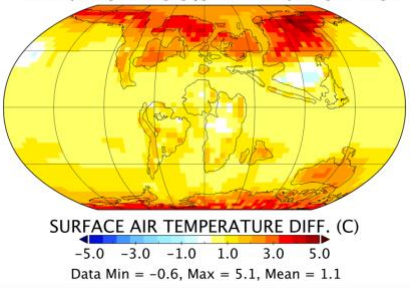

i) Annual precipitation for bare soil climatology

j) Annual precipitation for climatology with VBCs c, d, e

k) Annual precipitation difference of j) minus i).

https://doi.org/10.5194/egusphere-2026-4262
Preprint. Discussion started: 31 August 2026

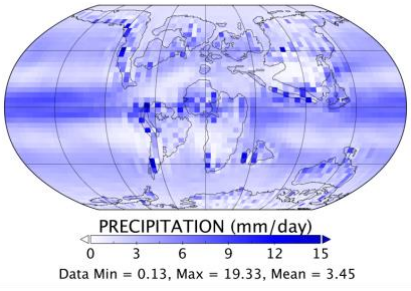

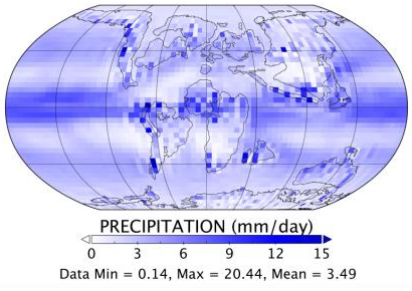

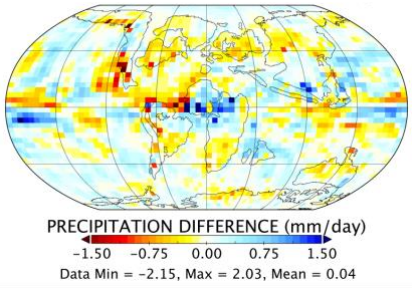

l) Ground albedo difference of climatology with VBCs c, d, e minus with bare soil.

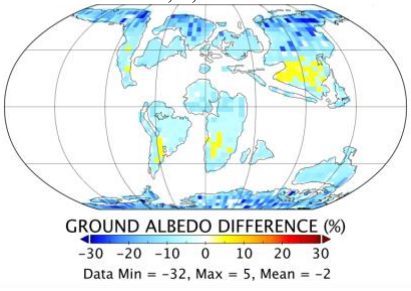

m) Updated Köppen-Geiger biome classes for 85 Mya Cretaceous climatology with VBCs c, d, e

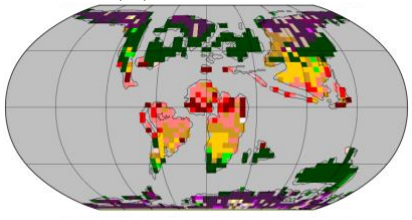

n) Updated paleo-vegetation dominant Ent cover types for 85 Mya climatology with VBCs c, d, e.

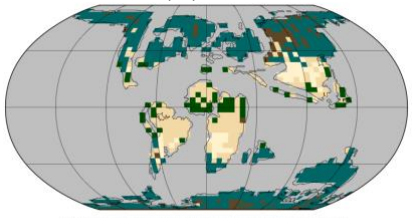

Figure 8. Two iterations of Cretaceous 85 Mya climatology and vegetation boundary conditions (VBCs) at 4° x 5° horizontal spatial resolution in the ROCKE-3D planet 2.0 planetary climate model: a) Köppen-Geiger biome classes given bare soil climatology, b) dominant Ent plant functional types (PFTs) if modern vegetation for classes in a) (complete subgrid cover fractions can be viewed in the Supplementary Material); c) paleo-vegetation dominant Ent PFTs for 85 Mya for a); d) canopy heights for 85 Mya for cover in b); e) maximum annual LAI for 85 Mya given cover in c); f) annual mean surface air temperature for bare soil climatology; g) annual mean surface air temperature for asynchronously equilibrated climatology from prescribing c, d, and e; h) change in annual mean surface air temperature of g) minus f); i) annual precipitation for bare soil climatology; j) annual precipitation for climatology with VBCs in c), d), and e); k) difference in annual precipitation of j) minus i); l) ground albedo difference from climatology using VBCs c), d), and e) minus bare soil climatology; m) Köppen-Geiger biome classes for the asynchronously updated climatology, showing n) northward expansion of shrubland and increase in deciduous needleleaf trees in the high latitudes due to vegetation warming the climate. See legends in Figure 1.

The mean annual surface air temperature for the bare soil climatology is show in Figure 8f. Prescribing the VBCs of Figures 8c, d, e, and the associated monthly LAI then results in a re-equilibrated climatology with a mean annual surface air temperature that is 1.1 Celsius warmer (Figure 8g). This warming extends over nearly the entire globe and with greatest warming in the high latitudes (Figure 8h). Precipitation between the bare soil climatology (Figure 8i) and the vegetated (Figure 8j) is significantly wetter than the modern (Figure 5d), with vegetation slightly increasing global precipitation, with regional decreases offset by increases particularly in central and northern Africa (Figure 8k).

The climate warming is directly due to overall decreases in the land surface albedo (including land snow/ice) with vegetation (Figure 8l). Generating the Köppen-Geiger classes with the climatology equilibrated with the VBCs of Figure 8c, d, e, and associated monthly LAI leads to slight expansion of evergreen broadleaf (tropical rainforest) into northern Africa, expansion of shrubland into the mid-latitudes, and slight expansion of deciduous needleleaf trees in Eurasia.Discussion

https://doi.org/10.5194/egusphere-2026-4262
Preprint. Discussion started: 31 August 2026

3.5 Efficacy of the Köppen-Geiger lookup table scheme

Our default "EntKGLUT" is derived from the decade 2001-2010, but the algorithms may be used to generate alternative LUTs from other observed climate and vegetation data. For example, a decadal climatology prior to apparent climate warming, such as 1980-1989, might better capture land cover patterns where there is inertia of vegetation change with climate change (however, satellite vegetation observations during this period are not as high quality). The year 2019 and later, when better forest height data started to become available, is a period already expressing vegetation change in the high latitudes, so a climatology straddling those years may be more appropriate.

The Köppen-Geiger classification scheme is not perfect, as noted in the Introduction. For example, because the Köppen-Geiger scheme utilizes only surface temperature and precipitation, it does not capture biomes whose climatology is influenced by other climate factors. We found that wetland areas which are fed by streamflow instead of precipitation in the Amazon and Congo Basins were classified instead to have extensive areas of forest, tall trees, and high LAI in Figure 1b, d, and e where the tropical biome classes Af and Am in Figure 1a fail to extend and where these wetland areas are instead classified as Aw, savannah. This contaminates the Aw classified cells with wetland vegetation in the LUT, but does not have a significant effect on the final LUT values. Comparing to the estimated map of Lane et al. (2023), boreal non-floodplain wetlands areas in Canada, the Nordic countries, and Russia, similarly show differences along those biome transition zones in albedo and biomass between E0 and E1. Also, our tool rests on the assumption that biomes in the past and future sort into the same climate classes (albeit not necessarily the same existing vegetation types) as the present. The further into the past, this is decreasingly likely, but given the limited fossil data for reconstructions our tool is expedient to predict broad PFTs in lieu of predicting vegetation with full DGVM simulations and their uncertain reliability. For near future climate in the next ~300 years, shifting biomes as consortia is a fair assumption at high latitudes, as has been observed over the past couple of decades (Magney & Pierrat, 2025)

Uncertainties in the source satellite data affect our results. Satellite-observed LAI saturates above ~5 (Fang et al. 2021), and the V005 product used here was capped at 7, and taking the mean of a biome's various distributions damps the maximum LAI to 5.5 in the regenerated VBCs. Rather than simple averaging, an improvement would be to quantify the seasonal timing, peak phase, and amplitude of LAI separately, common quantities to analyse satellite and model time series (Park & Jeong, 2021); climatological averages for these quantities would then provide a lookup table of a synthesized seasonal LAI, similar to an approach used in McDermid et al. (2019) to study sensitivity of climate to cropland LAI timing.

With regard to canopy heights, the estimates in Simard et al. (2011) do not resolve more precisely than 5 m, and we found their forest mean estimated heights to be too tall by as much as 6-8 m, compared to more recent data (Dubayah et al., 2021), leading to overestimated biomass. We plan to replace the over-estimated heights from ICESat/GLAS in Ent GVSD v1.0 with the more accurate canopy heights from GEDI and ICESat-2 (Saatchi & Favrichon, 2023), and allometric relations to height will be updated from recent analyses of the *Tallo* database (Grant et al., 2025; Jucker et al., 2022). These updates should greatly rectify the over-estimated forest biomass compared to when Ent uses the v1.0 boundary conditions.

https://doi.org/10.5194/egusphere-2026-4262
Preprint. Discussion started: 31 August 2026

Uncertainties in both data sources and estimating global vegetation biomass remain a current challenge, while extracting more nuanced estimates from the full information in new lidar satellite data remains an for research.

The KDE approach is quite accurate at identifying peaks in the frequency distributions of the VBCs that are not necessarily normally distributed (Figures S1-S3). However, biome types that span ecotones exhibit bimodal distributions of cover fraction, such as savannahs (As) and mixed ecosystems (Cfa drought-deciduous broadleaf trees) with grid cells at extreme ranges of those biomes. Some high latitude climates spanning tundra to forest may exhibit contamination of shrub or grass LAI by tree LAI in the MODIS data product (Dfb cold shrubs, Dfa C3 arctic grasses). In these cases, the KDE algorithm selected the most frequent peak for the LUT value. Overall, we found the KDE approach the most consistently effective at identifying justifiable LUT values, compared to simply selecting the average properties the grid cells.

The ground albedo underprediction in the Sahara and overprediction in the Australia interior was due to their both contributing to the average properties of the BWh ("Arid desert hot") Köppen-Geiger class but having different extents of bare soil and shrubland, yet these differences in the albedos were not large enough to alter the simulated regional climates. The Ent Köppen-Geiger classification of northern African excluded current croplands while interior Australia was classified as mostly shrubland and underpredicted bare ground exposure through sparse shrubs. The BWh biome-climate class also might simply span a range of bare soil to shrubland without significant atmospheric sensitivity to the different albedos in this hot, arid climate. Therefore, the albedo biases are a combination of the natural BWh range in the Köppen-Geiger classes and/or the climatological data used to do the classification and/or the deficiencies in the satellite-observed vegetation and derived maps in the Ent GVSD.

Despite the deficiencies in the Köppen-Geiger classification system, the simplified representation of VBCs generated from the LUT captured the compositional features of the detailed satellite VBCs to reproduce simulated modern climate, even improving the model's original global mean cold bias, and with no difference to global mean precipitation.

For climatological studies including a coupled carbon cycle, these biomass uncertainties do not impact the climate simulations. The change in canopy structure, however, would affect canopy radiative transfer, roughness lengths and coupling between the land surface and the atmosphere, such that replacing with shorter heights could alter the simulated climatologies. However, given our coupled climate test, we expect any new LUT generated should provide VBCs that do not bias simulated modern climates compared to simulations using the original satellite source data.

3.6 Paleo-vegetation prediction

A fossil reconstruction of Saward (1992) for the Late Cretaceous, Turonian-Maastrichtian (~93.9-66 Mya) is shown in Figure 9, which estimates an equatorial tropical mix of broadleaved evergreen trees and arid shrubs (a), grading toward the poles to paratropical evergreen broadleaf and evergreen needleleaf trees (conifers) in the mid-latitudes (b), then mixed evergreen and deciduous coniferous and broadleaf woodlands (c), and temperate mixed conifer/broadleaf deciduous forest in the high latitudes (d). The broad temporal range allows for potential cover by broadleaf deciduous trees, while our narrowly selected time of 85 Mya does not. For predicting the VBCs with the EntKGLUT, the ROCKE-3D simulated climatology is

https://doi.org/10.5194/egusphere-2026-4262
Preprint. Discussion started: 31 August 2026

too cold at the higher latitudes for temperate vegetation, predicting boreal climates, Df. This could be partly because the simulation is based on a bare soil climatology, which could be colder due to both increased dust (Liu et al., 2020) and lighter albedo compared to if vegetation cover were present at the high latitudes. However, a known issue in Earth system model simulations of extremely warm climates is that the models fail to capture the low equator-to-pole temperature gradients suggested by paleoproxy data (Zhu et al., 2024 and references therein). As a result, the vegetation cover map predicted by the EntKGLUT and paleo-vegetation replacement algorithms, with both the preliminary bare soil climatology and warmer vegetated climatology, shifts the Saward (1992) forest and woodland biomes southward. In the northern high latitudes, the Köppen-Geiger boreal climate, Df, results in evergreen and deciduous needleleaf forests, whereas the fossil reconstruction over the broader time period estimates these latitudes as being temperate mixed conifer/broadleaf deciduous forest. The modern Ent PFTs in these biome classes, however, show mixed forest well to the poles. The full subgrid cover fractions for the EntKGLUT predictions can be viewed in the Supplementary Figures S1 and in the netcdf files S10.

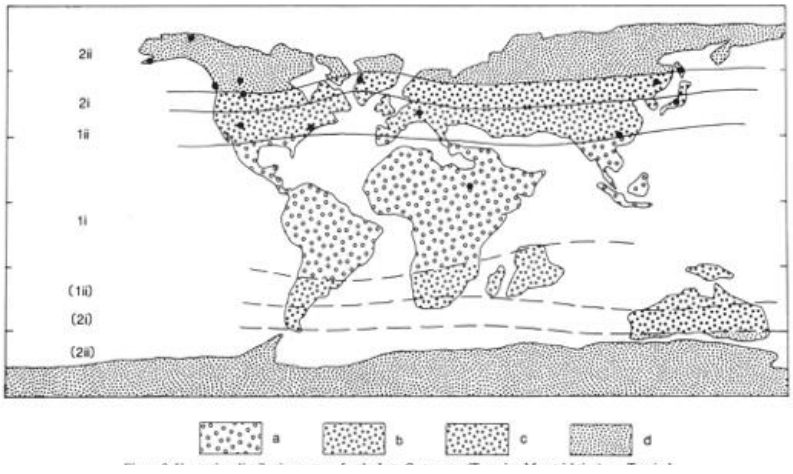

a = Tropical vegetation; broad-leaved evergreen forest/shrubland.

b = Paratropical vegetation; broad-leaved (and coniferous) evergreen forest/woodland.

c = Paratemperate vegetation; coniferous and/or broad-leaved semi-deciduous/evergreen forest/woodland.

d = Temperate vegetation; coniferous and/or broad-leaved deciduous forest

Figure 9. Fossil reconstruction of vegetation distribution pattern for the Late Cretaceous (Turonian-Maastrichtian). Source: Saward et al. (1992). Reproduced under the Geological Society of American's "Fair Use" copyright policy.

The Saward (1992) reconstruction for ~93.9-66 Mya also allows for deciduous broadleaf trees much earlier than the emergence time at 66 Mya that we specified based on Wolfe (1987). So, our paleo-vegetation replacement of the northern forests only has evergreen and deciduous needleleaf trees at 85 Mya. A more recent analysis of the fossil record by Vajda and Bercovici (2014) confirms, at least, that deciduousness existed by the end of the Cretaceous. They also observe: "The environment was clearly forested but the mix of deciduous and evergreen elements with palm trees and conifers, and extremely

https://doi.org/10.5194/egusphere-2026-4262
Preprint. Discussion started: 31 August 2026

high diversity of angiosperms with lobed leaves...do not have any close modern analog." The Ent vegetation model does not have palm trees as a PFT, but for the broad biophysical features of vegetation, it remains for future research to ascertain whether the represented PFTs are sufficient for climate modeling.

The phylogeny of vegetation is subject to ranges of estimates for the origins of different taxa and updates with new fossil discoveries and molecular clock estimates. Therefore, our paleo-vegetation algorithms, with dating estimates from recent literature, are certainly material for future revisions. Our VBC tool presented here does not predict vegetation distributions prior to ~150-200 Mya, because the Ent TBM does not have comparable plant functional types for some of the earlier plant types. Photosynthetic organisms on land could have included cyanobacterial crusts during the Proterozoic as early as 1 Gya; bryophytes emerging in the middle Ordovician (~470 Mya); vascular plants by the middle Devonian (~390 Mya), with ferns by the late Devonian, and cycads in the mid-late Carboniferous (~320 Mya). Modifying the Ent TBM to include these plant types would requires alternative physiological and allometric parameterizations for these types. However, predicting their spatial distributions and seasonality could not be based on derivation from global satellite data and Köppen-Geiger biome classification, but would require either full vegetation change dynamics or other correlational approaches, derived from their environmental physiology in the literature and possibly high-resolution air-borne remote sensing and meteorological data.

4 Conclusions

Our Köppen-Geiger PFT vegetation boundary conditions algorithms provide a useful utility for generating the broad patterns of VBCs for simulating biophysics in GCMs in alternative climates, when the models or science question do not require full biogeochemical and ecological dynamics. The tool can be used asynchronously coupled with GCMs if equilibration of vegetation cover change is desired. The algorithms could even be programmed online; this would necessitate the GCM internally collecting long-term running means of monthly surface temperature and precipitation statistics. Although our PFTs are based on one DGVM, the Ent Terrestrial Biosphere Model, the Ent model's classes are common enough among other DGVMs, such that the generated VBCs can be translated to other PFTs for use in other models.

For the general practice of applying the EntKGLUT to generate VBC's, we observe the following. That our experiment closely reproduces Modern simulated climate with reproduced VBCs leads us to conclude that our LUT tool will produce Köppen-Geiger biome maps and VBCs that are sufficiently accurate for characterizing a given climatology. If the goal is to have accurate VBCs for a known time period but without having sufficient climate statistics to use the Köppen -Geiger classification algorithms, one could try to construct a Köppen-Geiger biome map through qualitative judgment and apply the EntKGLUT to that biome map to generate VBCs. If the goal is to simulate vegetation-climate feedbacks with vegetation predicted from the online climate through asynchronous coupling, then, as with all coupled ESM-DGVM simulations, one must be well aware of the climate model's biases. Finally, we have yet to see if replacing our bare soil initial Cretaceous climate simulation with the VBCs will help warm the climate in the high latitudes. This climatology is part of an initialization for an experiment for

https://doi.org/10.5194/egusphere-2026-4262
Preprint. Discussion started: 31 August 2026

another ROCKE-3D study, which will involve asynchronous coupling of the EntKGLUT+paleo predicted VBCs with the atmospheric model. Future work will describe the final VBCs equilibrated with the simulated Cretaceous climate.

Future versions of the Ent GVSD are planned to span the entire MODIS record over 2001-2025/2026, to provide more statistical robustness in quantifying climatological averages of monthly LAI and uncertainty in PFT identification. We may in addition add biome classifications of MODIS monthly surface albedos and of soil albedos derived from MODIS (Carrer et al., 2014). The Trewartha modifications to the Köppen-Geiger system (Belda et al., 2014) could be added to improve the biome classifications and VBCs statistics in the mid-latitudes. The paleo-vegetation algorithms can certainly be more nuanced, such as accounting for the continent where certain PFTs first emerged and spread. Additional PFTs for the Jurassic and earlier (> ~145 Mya) would be of interest, such as cycads and ferns. Finally, our tool natural affords the opportunity for GCM studies with asynchronous coupling with the EntKGLUT VBCs to equilibrate the cover fractions with climate and to investigate the impact of vegetation feedbacks to climate in time periods very different from the modern.

5 Data sets and code

The data sets and scripts for generating the Köppen-Geiger-based lookup tables of VBCs are archived at zenodo.org, doi: 10.5281/zenodo.17917285 (Kiang et al., 2026). A repository for community contributions is available on github at https://github.com/ent-tbm/ent_kglut.git. We welcome community contributions to add variations on the algorithms for generating the modern LUT and especially to add to and refine the paleo-vegetation algorithms, for which there can be numerous versions addressing debates and new discoveries.

6 Author contributions

NYK, project supervision and conceptualization, Köppen-Geiger classification codes, satellite data sets, conceptualization of LUT generation and climate simulations, original manuscript writing and editing. CYJL, conceptualization and code development for KDE algorithms, LUT generation, and paleo-vegetation timing and spread algorithms, ModelE modern climate simulations, writing and editing. LES, Cretaceous topographic boundary conditions, writing editing. SG, ROCKE-3D simulations of Cretaceous climate, writing and editing.

7 Acknowledgements

The authors wish to thank Ondrea Clarkson and Jeffrey Jonas for Cretaceous continental boundary files for visualization. We also thank Heather Graham for early advising on paleo-vegetation temporal distributions. The CYJL and NYK were supported by the NASA Modeling, Analysis, and Prediction (MAP) Program and the GSFC Sellers Exoplanet Environments Collaboration (SEEC) Internal Scientist Funding Model (ISFM), which is supported by NASA's Planetary, Astrophysics and Heliophysics Science Divisions' Research Program. NYK, SG, LES, and OC were supported by the NASA Interdisciplinary

https://doi.org/10.5194/egusphere-2026-4262
Preprint. Discussion started: 31 August 2026

Consortia for Astrobiology Research (ICAR); NASA Earth and Planetary Science Division Research Programs, through Internal Scientist Funding Model (ISFM) work package ROCKE-3D (22-ICAR22_2-0015) at the Goddard Institute for Space Studies. Resources supporting this work were provided by the NASA High-End Computing (HEC) Program through the NASA Center for Climate Simulation (NCCS) at Goddard Space Flight Center. The results reported herein benefitted from collaborations and/or information exchange between NASA's Nexus for Exoplanet System Science (NExSS) and Network for Life Detection (NfoLD) research coordination networks sponsored by NASA's Science Mission Directorate.

8 Conflict of Interest Statement

The authors have no conflict of interest to declare.

https://doi.org/10.5194/egusphere-2026-4262
Preprint. Discussion started: 31 August 2026

Appendix A

A.1 Formatting vegetation boundary condition files for input to ModelE

The Ent GVSD v1.0 was derived from regridding all source data to 0.5° x 0.5°. To make any VBCs suitable for the Ent TBM, whether off-line or coupled in ModelE, additional processing steps are done to produce the input files for the ModelE grid. To allow transient historical simulations with historical crop cover specified separately such as from the Land-Use Harmonization data sets (Hurtt et al., 2020), a natural vegetation-only cover file is created by scaling out the crop cover; this natural vegetation cover is proportionately rescaled with historical crop cover so that all vegetation fractions and bare soil sum to 1 for the portion of the grid cell with soil hydrology. The mapped data are then regridded to the GCM grid of 2.5° x 2.0°. Because of mismatches between satellite data products or changing historical crop cover, there can be grid cells where the land cover type is non-zero but the LAI or height have no specified value. To ensure all non-zero cover has non-zero vegetation structure, rather than discard those cover fractions that do not have matching VBC's, instead we produce an "extended" version of the VBCs in which the LAI or height values (but not cover) are extended along their same latitude to grid cells that lack such VBCs. In general, such grid cells are small fraction and tend to have cover fractions of zero or very small values for that PFT. The code for producing these "extended" versions is available in a repository of scripting tools for the Ent TBM and made publicly available.

A.2 Köppen-Geiger classes

We classify 30 Köppen-Geiger biomes, represented in the first 30 rows of Table A 1, as described in the main text.

Table A 1. Köppen-Geiger biome/climate classes, with color scheme from http://koeppen-geiger.vu-wien.ac.at/. The "Unknown" biomes are those that did not match the any biomes in the classification scheme of Kottek et al. (2006); these are described in the Appendix text.

	Class	Color	Description
1	Af	dark red	Equatorial rainforest
2	Am	bright red	Equatorial monsoon
3	As	dark pink	Equatorial savannah with dry summer
4	Aw	pale pink	Equatorial savannah with dry winter
5	BWk	pale yellow	Arid desert cold
6	BWh	medium yellow	Arid desert hot
7	BSk	cool brown	Arid steppe cold steppe
8	BSh	warm yellow-brown	Arid steppe hot
9	Csa	bright green	Warm temperate with dry hot summer
10	Csb	yellow green	Warm temperate with dry warm summer
11	Csc	yellower green	Warm temperate with dry cool summer and cold winter
12	Csd		Not a known climate
13	Cwa	warm brown	Warm temperate with dry winter and hot summer
14	Cwb	medium cool brown	Warm temperate with dry winter and warm summer
15	Cwc	dark brown	Warm temperate with dry cold winter and cool summer
16	Cwd		Not a known climate
17	Cfa	dark green	Warm temperate fully humid with hot summer
18	Cfb	medium green	Warm temperate fully humid with warm summer
19	Cfc	medium vivid green	Warm temperate fully humid with cool summer and cold winter
20	Cfd		Not a known climate

https://doi.org/10.5194/egusphere-2026-4262
Preprint. Discussion started: 31 August 2026

21	Dsa	magenta	Snow with dry hot summer
22	Dsb	pale magenta	Snow with dry warm summer
23	Dsc	paler magenta	Snow with dry cool summer and cold winter
24	Dsd	pale pink-grey	Snow with dry summer extremely continental
25	Dwa	pale grey purple	Snow with dry winter and hot summer
26	Dwb	medium grey purple	Snow with dry winter and warm summer
27	Dwc	grey purple	Snow with dry cold winter and cool summer
28	Dwd	deep grey purple	Snow with dry winter extremely continental
29	Dfa	black purple	Snow fully humid with hot summer
30	Dfb	red purple	Snow fully humid with warm summer
31	Dfc	bright purple	Snow fully humid with cool summer and cold winter
32	Dfd	red fuchsia	Snow fully humid extremely continental
33	EF	grey blue	Polar frost
34	ET	turquoise	Polar tundra
35	UA	light gray 1	Unknown equatorial cool. Never generated.
36	UAu	light gray 2	Unknown equatorial dry.
37	UB	light gray 3	Unknown arid. Never generated.
38	UE	light gray 4	Unknown polar. Never generated.
39	Ufu	light gray 5	Unknown warm temp. with snow. Never generated.
40	Uuu	light gray 6	No data.

The "Unknown" biomes in Table A 1 are error-catching classes that should not otherwise be generated if the classifying codes are called correctly. Only UAu can possibly be generated, as an "Unknown equatorial dry" climate type that does not match the any biomes in the classification scheme. For UAu, the mean annual temperature is equatorial (≥18 C), but the precipitation does not satisfy the ranges for biomes Af, Am, As, or Aw. There are 4 pixels that are UAu.

A.3 Default modern climate Ent Köppen-Geiger Lookup Table ("EntKGLUT")

Table A 2 shows the default lookup table, "EntKGLUT" giving cover fractions for each Ent cover type within each Köppen-Geiger biome type. All values are specified to 2 decimal places. The lookup table is also provided as a netcdf file in the Supplementary Material.

Table A 2. Lookup table "EntKGLUT" v1.0 of Ent PFT and bare soil cover fractions by Köppen-Geiger biome. This table is also provided in an Excel spreadsheet in the Supplementary Material S7, and in a netcdf file in Supplementary Material S10.

Ent cover type	evergreen broadleaf tree	evergreen needleleaf tree	cold deciduous broadleaf tree	drought deciduous broadleaf	deciduous needleleaf	cold adapted shrub	arid adapted shrub	C3 grass perennial	C4 grass	C3 grass	arctic C3 grass	crops herb	bright bare soil	dark bare soil
Af	1	0	0	0	0	0	0	0	0	0	0	0	0	0
Am	0.8	0.1	0	0	0	0	0	0	0.1	0	0	0	0	0
As	0.14	0	0	0	0	0	0.52	0	0.34	0	0	0	0	0

https://doi.org/10.5194/egusphere-2026-4262
Preprint. Discussion started: 31 August 2026

Ent cover type	evergreen broadleaf tree	evergreen needleleaf tree	cold deciduous broadleaf tree	drought deciduous broadleaf	deciduous needleleaf	cold adapted shrub	arid adapted shrub	C3 grass perennial	C4 grass	C3 grass	arctic C3 grass	crops herb	bright bare soil	dark bare soil
Aw	0.21	0	0	0.18	0	0	0.34	0	0.27	0	0	0	0	0
BWk	0	0	0	0	0	0	0.31	0.15	0	0	0	0	0.26	0.28
BWh	0	0	0	0	0	0	0.36	0	0	0	0	0	0.45	0.19
BSk	0	0	0	0	0	0	0.4	0.49	0	0.11	0	0	0	0
BSh	0	0	0	0	0	0	0.68	0	0.32	0	0	0	0	0
Csa	0	0.1	0	0	0	0	0.52	0.15	0	0.23	0	0	0	0
Csb	0.13	0.34	0	0	0	0	0.36	0.17	0	0	0	0	0	0
Csc	0	0.16	0	0	0	0.13	0.58	0.13	0	0	0	0	0	0
Csd	0	0	0	0	0	0	0	0	0	0	0	0	0	0
Cwa	0.13	0	0.14	0.24	0	0	0.26	0.09	0.14	0	0	0	0	0
Cwb	0.1	0.15	0	0.1	0	0	0.26	0.28	0	0.11	0	0	0	0
Cwc	0	0	0	0	0	0	0.33	0.11	0	0.56	0	0	0	0
Cwd	0	0	0	0	0	0	0	0	0	0	0	0	0	0
Cfa	0	0.16	0.39	0	0	0	0.1	0.16	0.19	0	0	0	0	0
Cfb	0.2	0.24	0.33	0	0	0	0.08	0.15	0	0	0	0	0	0
Cfc	0.14	0.28	0	0	0	0	0.39	0.19	0	0	0	0	0	0
Cfd	0	0	0	0	0	0	0	0	0	0	0	0	0	0
Dsa	0	0	0	0	0	0	0	0.9	0	0.1	0	0	0	0
Dsb	0	0.33	0	0	0	0	0	0.67	0	0	0	0	0	0
Dsc	0	0.25	0	0	0	0.65	0	0	0	0	0.1	0	0	0
Dsd	0	0	0	0	0	0.85	0	0	0	0	0.15	0	0	0
Dwa	0	0	0.63	0	0	0	0	0.27	0	0.1	0	0	0	0
Dwb	0	0	0.64	0	0	0	0	0.36	0	0	0	0	0	0
Dwc	0	0.16	0.09	0	0.3	0.23	0	0.13	0	0	0.09	0	0	0
Dwd	0	0	0	0	0.25	0.75	0	0	0	0	0	0	0	0
Dfa	0	0.17	0.34	0	0	0	0	0.49	0	0	0	0	0	0
Dfb	0	0.41	0.4	0	0	0	0	0.19	0	0	0	0	0	0
Dfc	0	0.45	0	0	0.13	0.42	0	0	0	0	0	0	0	0
Dfd	0	0.09	0	0	0.13	0.78	0	0	0	0	0	0	0	0
EF	0	0	0	0	0	0.13	0	0	0	0	0	0	0.71	0.16
ET	0	0	0	0	0	0.61	0	0.12	0	0	0.27	0	0	0
UA	0	0	0	0	0	0	0	0	0	0	0	0	0.3	0.7
UAu	0	0	0	0	0	0	0	0	0	0	0	0	0.3	0.7
UB	0	0	0	0	0	0	0	0	0	0	0	0	0.6	0.4
UE	0	0	0	0	0	0	0	0	0	0	0	0	0.82	0.18
Ufu	0	0	0	0	0	0	0	0	0	0	0	0	0.82	0.18
Uuu	0	0	0	0	0	0	0	0	0	0	0	0	0.6	0.4

https://doi.org/10.5194/egusphere-2026-4262
Preprint. Discussion started: 31 August 2026

References

Anav, A., Friedlingstein, P., Beer, C., Ciais, P., Harper, A., Jones, C., Murray-Tortarolo, G., Papale, D., Parazoo, N. C., Peylin, P., Piao, S. L., Sitch, S., Viovy, N., Wiltshire, A., & Zhao, M. S. (2015). Spatiotemporal patterns of terrestrial gross primary production: A review. *Reviews of Geophysics*, *53*(3), 785–818. https://doi.org/10.1002/2015rg000483

Argles, A. P. K., Moore, J. R., & Cox, P. M. (2022). Dynamic Global Vegetation Models: Searching for the balance between demographic process representation and computational tractability. *PLOS Climate*, *1*(9), e0000068. https://doi.org/10.1371/journal.pclm.0000068

Beck, H. E., Zimmermann, N. E., McVicar, T. R., Vergopolan, N., Berg, A., & Wood, E. F. (2018). Present and future Köppen-Geiger climate classification maps at 1-km resolution. *Scientific Data*, *5*(1), 180214. https://doi.org/10.1038/sdata.2018.214

Belda, M., Holtanová, E., Halenka, T., & Kalvová, J. (2014). Climate classification revisited: from Köppen to Trewartha. *Climate Research*, *59*, 1–13. https://doi.org/https://doi.org/10.3354/cr01204

Brierley, C. M., Zhao, A., Harrison, S. P., Braconnot, P., Williams, C. J. R., Thornalley, D. J. R., Shi, X., Peterschmitt, J. Y., Ohgaito, R., Kaufman, D. S., Kageyama, M., Hargreaves, J. C., Erb, M. P., Emile-Geay, J., D'Agostino, R., Chandan, D., Carré, M., Bartlein, P. J., Zheng, W.,…Abe-Ouchi, A. (2020). Large-scale features and evaluation of the PMIP4-CMIP6 midHolocene simulations. *Clim. Past*, *16*(5), 1847–1872. https://doi.org/10.5194/cp-16-1847-2020

Burgener, L., Hyland, E., Reich, B. J., & Scotese, C. (2023). Cretaceous climates: Mapping paleo-Köppen climatic zones using a Bayesian statistical analysis of lithologic, paleontologic, and geochemical proxies. *Palaeogeography, Palaeoclimatology, Palaeoecology*, *613*, 111373. https://doi.org/https://doi.org/10.1016/j.palaeo.2022.111373

Carrer, D., Meurey, C., Ceamanos, X., Roujean, J. L., Calvet, J. C., & Liu, S. (2014). Dynamic mapping of snow-free vegetation and bare soil albedos at global 1 km scale from 10-year analysis of MODIS satellite products. *Remote Sensing of Environment*, *140*, 420–432. https://doi.org/https://doi.org/10.1016/j.rse.2013.08.041

Charney, J., Stone, P. H., & Quirk, W. J. (1975). Drought in the Sahara: A Biogeophysical Feedback Mechanism. *Science*, *187*(4175), 434–435. https://doi.org/doi:10.1126/science.187.4175.434

Chen, W. Z., Zhu, D., Ciais, P., Huang, C. J., Viovy, N., & Kageyama, M. (2019). Response of vegetation cover to CO2 and climate changes between Last Glacial Maximum and pre-industrial period in a dynamic global vegetation model. *Quaternary Science Reviews*, *218*, 293–305. https://doi.org/10.1016/j.quascirev.2019.06.003

Cheng, L., Zhang, L., Wang, Y.-P., Canadell, J. G., Chiew, F. H. S., Beringer, J., Li, L., Miralles, D. G., Piao, S., & Zhang, Y. (2017). Recent increases in terrestrial carbon uptake at little cost to the water cycle. *Nature Communications*, *8*(1), 110. https://doi.org/10.1038/s41467-017-00114-5

Crane, P. R., & Lidgard, S. (1989). Angiosperm Diversification and Paleolatitudinal Gradients in Cretaceous Floristic Diversity. *Science*, *246*(4930), 675–678. https://doi.org/10.1126/science.246.4930.675

Defries, R. S., Field, C. B., Fung, I., Justice, C. O., Los, S. O., Matson, P. A., Matthews, E., Mooney, H. A., Potter, C., Prentice, K. C., Sellers, P. J., Townshend, J., Tucker, C. J., Ustin, S. L., & Vitousek, P. (1995). Mapping the land surface for global atmosphere-biosphere models - toward continuous distributions of vegetation's functional properties. *Journal of Geophysical Research - Atmospheres*, *100*(D10), 20,867–820,882. https://doi.org/ https://doi.org/10.1029/95JD01536

Dorman, J. L., & Sellers, P. J. (1989). A Global Climatology of Albedo, Roughness Length and Stomatal Resistance for Atmospheric General Circulation Models as Represented by the Simple Biosphere Model (SiB). *Journal of Applied Meteorology and Climatology*, *28*(9), 833–855.

Dubayah, R. O., Armston, J., Healey, S. P., Bruening, J. M., Patterson, P. L., Kellner, J. R., Duncanson, L., Saarela, S., Ståhl, G., Yang, Z., Tang, H., Blair, J. B., Fatoyinbo, L., Goetz, S., Hancock, S., Hansen, M., Hofton, M., Hurtt, G., & Luthcke, S. (2022). GEDI launches a new era of biomass inference from space. *Environmental Research Letters*, *17*(9), 095001. https://doi.org/10.1088/1748-9326/ac8694

https://doi.org/10.5194/egusphere-2026-4262
Preprint. Discussion started: 31 August 2026

Dubayah, R. O., Armston, J., Healey, S. P., Yang, Z., Patterson, P. L., Saarela, S., Stahl, G., Duncanson, L., & Kellner, J. R. (2022). *GEDI L4B Gridded Aboveground Biomass Density, Version 2* (ORNL DAAC, Oak Ridge, Tennessee, USA. .

Dubayah, R. O., Luthcke, S. B., Sabaka, T. J., Nicholas, J. B., Preaux, S., & Hofton, M. A. (2021). GEDI L3 Gridded Land Surface Metrics, Version 2. In: ORNL Distributed Active Archive Center.

Edwards, E. J., Osborne, C. P., Strömberg, C. A. E., Smith, S. A., Consortium, C. G., Bond, W. J., Christin, P.-A., Cousins, A. B., Duvall, M. R., Fox, D. L., Freckleton, R. P., Ghannoum, O., Hartwell, J., Huang, Y., Janis, C. M., Keeley, J. E., Kellogg, E. A., Knapp, A. K., Leakey, A. D. B.,…Tipple, B. (2010). The Origins of C4 Grasslands: Integrating Evolutionary and Ecosystem Science. *Science*, *328*(5978), 587–591. https://doi.org/10.1126/science.1177216

Favrichon, S., Lee, J., Yang, Y., Dalagnol, R., Wagner, F., Sagang, L. B., & Saatchi, S. (2025). Monitoring changes of forest height in California [Original Research]. *Frontiers in Remote Sensing*, *Volume 5 - 2024*. https://doi.org/10.3389/frsen.2024.1459524

Feng, T., Duncanson, L., Montesano, P., Hancock, S., Minor, D., Guenther, E., & Neuenschwander, A. (2023). A systematic evaluation of multi-resolution ICESat-2 ATL08 terrain and canopy heights in boreal forests. *Remote Sensing of Environment*, *291*, 113570. https://doi.org/https://doi.org/10.1016/j.rse.2023.113570

Fisher, R. A., & Koven, C. D. (2020). Perspectives on the Future of Land Surface Models and the Challenges of Representing Complex Terrestrial Systems. *Journal of Advances in Modeling Earth Systems*, *12*(4), Article e2018MS001453. https://doi.org/10.1029/2018ms001453

Fisher, R. A., Koven, C. D., Anderegg, W. R. L., Christoffersen, B. O., Dietze, M. C., Farrior, C. E., Holm, J. A., Hurtt, G. C., Knox, R. G., Lawrence, P. J., Lichstein, J. W., Longo, M., Matheny, A. M., Medvigy, D., Muller-Landau, H. C., Powell, T. L., Serbin, S. P., Sato, H., Shuman, J. K.,…Moorcroft, P. R. (2018). Vegetation demographics in Earth System Models: A review of progress and priorities. *Global Change Biology*, *24*(1), 35–54. https://doi.org/10.1111/gcb.13910

Friedl, M. A., McIver, D. K., Hodges, J. C. F., Zhang, X. Y., Muchoney, D., Strahler, A. H., Woodcock, C. E., Gopal, S., Schneider, A., Cooper, A., Baccini, A., Gao, F., & Schaaf, C. (2002). Global land cover mapping from MODIS: algorithms and early results [Article]. *Remote Sensing of Environment*, *83*(1-2), 287–302.

Friedl, M. A., Sulla-Menashe, D., Tan, B., Schneider, A., Ramankutty, N., Sibley, A., & Huang, X. M. (2010). MODIS Collection 5 global land cover: Algorithm refinements and characterization of new datasets [Article]. *Remote Sensing of Environment*, *114*(1), 168–182. https://doi.org/10.1016/j.rse.2009.08.016

Friedlingstein, P., Cox, P., Betts, R., Bopp, L., Von Bloh, W., Brovkin, V., Cadule, P., Doney, S., Eby, M., Fung, I., Bala, G., John, J., Jones, C., Joos, F., Kato, T., Kawamiya, M., Knorr, W., Lindsay, K., Matthews, H. D.,…Zeng, N. (2006). Climate-carbon cycle feedback analysis: Results from the (CMIP)-M-4 model intercomparison. *Journal of Climate*, *19*(14), 3337–3353.

Friedlingstein, P., Meinshausen, M., Arora, V. K., Jones, C. D., Anav, A., Liddicoat, S. K., & Knutti, R. (2014). Uncertainties in CMIP5 Climate Projections due to Carbon Cycle Feedbacks. *Journal of Climate*, *27*(2), 511–526. https://doi.org/10.1175/jcli-d-12-00579.1

Friedlingstein, P., O'Sullivan, M., Jones, M. W., Andrew, R. M., Hauck, J., Landschützer, P., Le Quéré, C., Li, H., Luijkx, I. T., Olsen, A., Peters, G. P., Peters, W., Pongratz, J., Schwingshackl, C., Sitch, S., Canadell, J. G., Ciais, P., Jackson, R. B., Alin, S. R.,…Zeng, J. (2025). Global Carbon Budget 2024. *Earth Syst. Sci. Data*, *17*(3), 965–1039. https://doi.org/10.5194/essd-17-965-2025

Friend, A. D., Arneth, A., Kiang, N. Y., Lomas, M., Ogée, J., Rödenbeck, C., Running, S. W., Santaren, J.-D., Sitch, S., Viovy, N., Woodward, F. I., & Zaehle, S. (2007). FLUXNET and modelling the global carbon cycle. *Global Change Biology*, *13*(3), 610–633. https://doi.org/https://doi.org/10.1111/j.1365-2486.2006.01223.x

Gallaher, T., Peterson, P., Soreng, R., Zuloaga, F., Li, D., Clark, L., Tyrrell, C., Welker, C., Kellogg, E., & Teisher, J. (2022). Grasses through space and time: An overview of the biogeographical and macroevolutionary history of Poaceae. *Journal of Systematics and Evolution*, *60*(3), 522–569. https://doi.org/10.1111/jse.12857

Grant, I., Ni-Meister, W., & Kiang, N. Y. (2025). Multiscale analysis of global variation in tree allometric relationships: parameter sets for global vegetation models. *Environmental Research: Ecology*.

Gu, L., Baldocchi, D., & Kiang, N. (2000). FLUXNET Evaluates "Breathing patterns" of diverse ecosystems. *Eos, Transactions American Geophysical Union*, *81*(47), 565–570.

https://doi.org/10.5194/egusphere-2026-4262
Preprint. Discussion started: 31 August 2026

Hansen, J., Russell, G., Rind, D., Stone, P., Lacis, A., Lebedeff, S., Ruedy, R., & Travis, L. (1983). Efficient three-dimensional global models for climate studies: Models I and II. *Monthly Weather Review*, *111*(4), 609–662. https://doi.org/https://doi.org/10.1175/1520-0493(1983)111<0609:ETDGMF>2.0.CO;2

Harris, I. (2014). *CRU TS3.22: Climatic Research Unit (CRU) Time-Series (TS) Version 3.22 of High Resolution Gridded Data of Month-by-month Variation in Climate (1901-2013)* (NERC British Atmospheric Data Centre. https://doi.org/10.5285/18BE23F8-D252-482D-8AF9-5D6A2D40990C

Harris, I., Jones, P. D., Osborn, T. J., & Lister, D. H. (2014). Updated high-resolution grids of monthly climatic observations - the CRU TS3.10 Dataset. *International Journal of Climatology*, *34*(3), 623–642. https://doi.org/10.1002/joc.3711

Haverd, V., Lovell, J. L., Cuntz, M., Jupp, D. L. B., Newnham, G. J., & Sea, W. (2012). The Canopy Semi-analytic P-gap And Radiative Transfer (CanSPART) model: Formulation and application. *Agricultural and Forest Meteorology*, *160*, 14–35. https://doi.org/10.1016/j.agrformet.2012.01.018

Haxeltine, A., & Prentice, I. C. (1996). BIOME3: An equilibrium terrestrial biosphere model based on ecophysiological constraints, resource availability, and competition among plant functional types [Proceedings Paper]. *Global Biogeochemical Cycles*, *10*(4), 693–709.

Herman, A. B., & Sokolova, A. B. (2016). Late Cretaceous Kholokhovchan Flora of Northeastern Asia: Composition, age and fossil plant descriptions. *Cretaceous Research*, *59*, 249–271. https://doi.org/https://doi.org/10.1016/j.cretres.2015.11.008

Herold, N., Buzan, J., Seton, M., Goldner, A., Green, J. A. M., Müller, R. D., Markwick, P., & Huber, M. (2014). A suite of early Eocene (~55 Ma) climate model boundary conditions. *Geoscience Model Development*, *7*, 2077–2090.

Hersbach, H., Bell, B., Berrisford, P., Hirahara, S., Horányi, A., Muñoz-Sabater, J., Nicolas, J., Peubey, C., Radu, R., Schepers, D., Simmons, A., Soci, C., Abdalla, S., Abellan, X., Balsamo, G., Bechtold, P., Biavati, G., Bidlot, J., Bonavita, M.,…Thépaut, J.-N. (2020). The ERA5 global reanalysis. *Quarterly Journal of the Royal Meteorological Society*, *146*(730), 1999–2049. https://doi.org/https://doi.org/10.1002/qj.3803

Holdridge, L. R. (1947). Determination of world plant formations from simple climatic data. *Science*, *105*(2727), 367–368. https://doi.org/10.1126/science.105.2727.367

Holdridge, L. R. (Ed.). (1967). *Life zone ecology*.

Huang, W., Zhang, L., Columbus, J., Hu, Y., Zhao, Y., Tang, L., Guo, Z., Chen, W., McKain, M., Bartlett, M., Huang, C., Li, D., Ge, S., & Ma, H. (2022). A well-supported nuclear phylogeny of Poaceae and implications for the evolution of C4 photosynthesis. *Molecular Plant*, *15*(4), 755–777. https://doi.org/10.1016/j.molp.2022.01.015

Hurrell, J. W., Hack, J. J., Shea, D., Caron, J. M., & Rosinski, J. (2008). A New Sea Surface Temperature and Sea Ice Boundary Dataset for the Community Atmosphere Model. *Journal of Climate*, *21*(19), 5145–5153. https://doi.org/https://doi.org/10.1175/2008JCLI2292.1

Hurtt, G. C., Chini, L., Sahajpal, R., Frolking, S., Bodirsky, B. L., Calvin, K., Doelman, J. C., Fisk, J., Fujimori, S., Klein Goldewijk, K., Hasegawa, T., Havlik, P., Heinimann, A., Humpenöder, F., Jungclaus, J., Kaplan, J. O., Kennedy, J., Krisztin, T., Lawrence, D.,…Zhang, X. (2020). Harmonization of global land use change and management for the period 850–2100 (LUH2) for CMIP6. *Geoscientific Model Development*, *13*(11), 5425–5464. https://doi.org/10.5194/gmd-13-5425-2020

Ito, G., Romanou, A., Kiang, N. Y., Faluvegi, G., Aleinov, I., Ruedy, R., Russell, G., Lerner, P., Kelley, M., & Lo, K. (2020). Global Carbon Cycle and Climate Feedbacks in the NASA GISS ModelE2.1. *Journal of Advances in Modeling Earth Systems*, *12*(10), e2019MS002030. https://doi.org/10.1029/2019MS002030

Jucker, T., Fischer, F. J., Chave, J., Coomes, D. A., Caspersen, J., Ali, A., Loubota Panzou, G. J., Feldpausch, T. R., Falster, D., Usoltsev, V. A., Adu-Bredu, S., Alves, L. F., Aminpour, M., Angoboy, I. B., Anten, N. P. R., Antin, C., Askari, Y., Muñoz, R., Ayyappan, N.,…Zavala, M. A. (2022). Tallo: A global tree allometry and crown architecture database. *Global Change Biology*, *28*(17), 5254–5268. https://doi.org/https://doi.org/10.1111/gcb.16302

Kageyama, M., Braconnot, P., Harrison, S. P., Haywood, A. M., Jungclaus, J. H., Otto-Bliesner, B. L., Peterschmitt, J. Y., Abe-Ouchi, A., Albani, S., Bartlein, P. J., Brierley, C., Crucifix, M., Dolan, A., Fernandez-Donado, L., Fischer, H., Hopcroft, P. O., Ivanovic, R. F., Lambert, F., Lunt, D. J.,…Zhou, T. (2018). The PMIP4 contribution to CMIP6 – Part 1: Overview and over-arching analysis plan. *Geoscientific Model Development*, *11*(3), 1033–1057. https://doi.org/10.5194/gmd-11-1033-2018

https://doi.org/10.5194/egusphere-2026-4262
Preprint. Discussion started: 31 August 2026

Kaplan, J. O., Bigelow, N. H., Prentice, I. C., Harrison, S. P., Bartlein, P. J., Christensen, T. R., Cramer, W., Matveyeva, N. V., McGuire, A. D., Murray, D. F., Razzhivin, V. Y., Smith, B., Walker, D. A., Anderson, P. M., Andreev, A. A., Brubaker, L. B., Edwards, M. E., & Lozhkin, A. V. (2003). Climate change and Arctic ecosystems: 2. Modeling, paleodata-model comparisons, and future projections. *Journal of Geophysical Research-Atmospheres*, *108*(D19), Article 8171. https://doi.org/10.1029/2002jd002559

Kelley, M., Schmidt, G. A., Nazarenko, L. S., Bauer, S. E., Ruedy, R., Russell, G. L., Ackerman, A. S., Aleinov, I., Bauer, M., Bleck, R., Canuto, V., Cesana, G., Cheng, Y., Clune, T. L., Cook, B. I., Cruz, C. A., Del Genio, A. D., Elsaesser, G. S., Faluvegi, G.,…Yao, M.-S. (2020). GISS-E2.1: Configurations and Climatology [https://doi.org/10.1029/2019MS002025]. *Journal of Advances in Modeling Earth Systems*, *12*(8), e2019MS002025. https://doi.org/https://doi.org/10.1029/2019MS002025

Kiang, N., Lui, C. Y. J., Sohl, L., & Guzewich, S. (2026). *Ent Köppen-Geiger LUT Tool v1.0* ([[Computer software]]. https://doi.org/https://doi.org/10.5281/zenodo.17917285

Kiang, N. Y., Aleinov, I., Schaaf, C., Sun, Q., Yao, T., Zhao, F., & Wang, Z. (in prep.). *The Ent Global Vegetation Structure Dataset: Version 1.0* [Technical Report].

Köppen, W. P. (1884). Die Wärmezonen der Erde, nach der Dauer der heissen, gemässigten und kalten Zeit, und nach der Wirkung der Wärme auf die organische Welt betrachtet. *Meteorologische Zeitschrift*.

Köppen, W. P., & Geiger, R. (1936). *Das geographische System der Klimate*. Berlin : Gebrüder Borntraeger.

Kottek, M., Grieser, J., Beck, C., Rudolf, B., & Rubel, F. (2006). World map of the Koppen-Geiger climate classification updated [Article]. *Meteorologische Zeitschrift*, *15*(3), 259–263. https://doi.org/10.1127/0941-2948/2006/0130

Lan, X., Thoning, K. W., & Dlugokencky, E. J. (2022). *Trends in globally-averaged CH4, N2O, and SF6 determined from NOAA Global Monitoring Laboratory measurements* (Version Version 2026-01). https://doi.org/https://doi.org/10.15138/P8XG-AA10

Lane, C. R., D'Amico, E., Christensen, J. R., Golden, H. E., Wu, Q., & Rajib, A. (2023). Mapping global non-floodplain wetlands. *Earth Syst. Sci. Data*, *15*(7), 2927–2955. https://doi.org/10.5194/essd-15-2927-2023

LePage, B., & Basinger, J. (1995). The evolutionary history of the genus Larix (Pinaceae). *United States Department of Agriculture, Forest Service, Intermountain Research Station, General Technical Report GTR-INT*, *319*, 19–29.

Liu, P., Liu, Y., Peng, Y., Lamarque, J.-F., Wang, M., & Hu, Y. (2020). Large influence of dust on the Precambrian climate. *Nature Communications*, *11*, 4427. https://doi.org/10.1038/s41467-020-18258-2

Liu, Y. J., Arens, N. C., & Li, C. S. (2007). Range change in Metasequoia: relationship to palaeoclimate. *Botanical Journal of the Linnean Society*, *154*(1), 115–127. https://doi.org/10.1111/j.1095-8339.2007.00597.x

Lunt, D. J., Dunkley Jones, T., Heinemann, M., Huber, M., LeGrande, A., Winguth, A., Loptson, C., Marotzke, J., Roberts, C. D., Tindall, J., Valdes, P., & Winguth, C. (2012). A model-data comparison for a multi-model ensemble of early Eocene atmosphere-ocean simulations: EoMIP. *Climate of the Past*, *8*(5), 1717–1736. https://doi.org/10.5194/cp-8-1717-2012

Ma, Y., Moorcroft, P. R., Wright, S. J., Rogers, A., Lamour, J., Davidson, K. J., Serbin, S. P., Detto, M., & Xu, X. (2025). Constraining Light-Driven Plasticity in Leaf Traits With Observations Improves the Prediction of Tropical Forest Demography, Structure, and Biomass Dynamics. *Journal of Geophysical Research: Biogeosciences*, *130*(6), e2025JG008814. https://doi.org/https://doi.org/10.1029/2025JG008814

Magney, T. S., & Pierrat, Z. A. (2025). Shifting equilibria in a warming boreal forest. *Proceedings of the National Academy of Sciences*, *122*(3), e2424669122. https://doi.org/10.1073/pnas.2424669122

Matthews, E. (1983). Global vegetation and land use: new high-resolution data bases for climate studies. *Journal of Climate and Applied Meteorology*, *22*, 474–487.

Matthews, E. (1984). *Prescription of land-surface boundary conditions in GISS GCM II: A simple method based on fine-resolution data bases* (86096). (NASA Technical Memo, Issue.

McDermid, S. S., Montes, C., Cook, B. I., Puma, M. J., Kiang, N. Y., & Aleinov, I. (2019). The Sensitivity of Land-Atmosphere Coupling to Modern Agriculture in the Northern Midlatitudes. *Journal of Climate*, *32*(2), 465–484. https://doi.org/10.1175/jcli-d-17-0799.1

Miller, R. L., Schmidt, G. A., Nazarenko, L. S., Bauer, S. E., Kelley, M., Ruedy, R., Russell, G. L., Ackerman, A. S., Aleinov, I., Bauer, M., Bleck, R., Canuto, V., Cesana, G., Cheng, Y., Clune, T. L., Cook, B., Cruz, C. A., Del Genio, A. D.,

https://doi.org/10.5194/egusphere-2026-4262
Preprint. Discussion started: 31 August 2026

Elsaesser, G. S.,…Yao, M. S. (2021). CMIP6 Historical Simulations (1850-2014) With GISS-E2.1. *Journal of Advances in Modeling Earth Systems*, *13*(1). https://doi.org/10.1029/2019MS002034

Moon, M., Richardson, A. D., O'Keefe, J., & Friedl, M. A. (2022). Senescence in temperate broadleaf trees exhibits species-specific dependence on photoperiod versus thermal forcing. *Agricultural and Forest Meteorology*, *322*, 109026. https://doi.org/https://doi.org/10.1016/j.agrformet.2022.109026

Moorcroft, P., Hurtt, G. C., & Pacala, S. W. (2001). A method for scaling vegetation dynamics: The Ecosystem Demography Model (ED). *Ecological Monographs*, *71*(4), 557–586. https://doi.org/DOI:10.1890/0012-9615(2001)071[0557:AMFSVD]2.0.CO;2

Myneni, R. B., Hoffman, S., Knyazikhin, Y., Privette, J. L., Glassy, J., Tian, Y., Wang, Y., Song, X., Zhang, Y., Smith, G. R., Lotsch, A., Friedl, M., Morisette, J. T., Votava, P., Nemani, R. R., & Running, S. W. (2002). Global products of vegetation leaf area and fraction absorbed PAR from year one of MODIS data [Article]. *Remote Sensing of Environment*, *83*(1-2), 214–231.

Neuenschwander, A., Guenther, E., White, J. C., Duncanson, L., & Montesano, P. (2020). Validation of ICESat-2 terrain and canopy heights in boreal forests. *Remote Sensing of Environment*, *251*, 112110. https://doi.org/https://doi.org/10.1016/j.rse.2020.112110

Neuenschwander, A., & Pitts, K. (2019). The ATL08 land and vegetation product for the ICESat-2 Mission. *Remote Sensing of Environment*, *221*, 247–259. https://doi.org/10.1016/j.rse.2018.11.005

Neuenschwander, A., Popescu, S., Nelson, R., Harding, D., Pitts, K., Robbins, J., Pederson, D., & Sheridan, R. (2019). *Ice, Cloud, and Land Elevation 1 Satellite 2 (ICESat-2) Algorithm Theoretical Basis Document (ATBD) for Land - Vegetation Along-Track Products (ATL08)*.

Ni-Meister, W., Yang, W. Z., & Kiang, N. Y. (2010). A clumped-foliage canopy radiative transfer model for a global dynamic terrestrial ecosystem model. I: Theory [Article]. *Agricultural and Forest Meteorology*, *150*(7-8), 881–894. https://doi.org/10.1016/j.agrformet.2010.02.009

Park, H., & Jeong, S. (2021). Leaf area index in Earth system models: how the key variable of vegetation seasonality works in climate projections. *Environmental Research Letters*, *16*(3), 034027. https://doi.org/10.1088/1748-9326/abe2cf

Parzen, E. (1962). On Estimation of a Probability Density Function and Mode, . *The Annals of Mathematical Statistics*, *33*(3), 1065–1076,.

Peel, M. C., Finlayson, B. L., & McMahon, T. A. (2007). Updated world map of the Köppen-Geiger climate classification. *Hydrol. Earth Syst. Sci.*, *11*(5), 1633–1644. https://doi.org/10.5194/hess-11-1633-2007

Piao, S., Liu, Q., Chen, A., Janssens, I. A., Fu, Y., Dai, J., Liu, L., Lian, X., Shen, M., & Zhu, X. (2019). Plant phenology and global climate change: Current progresses and challenges. *Glob Chang Biol*, *25*(6), 1922–1940. https://doi.org/10.1111/gcb.14619

Pohl, A., Wong Hearing, T., Franc, A., Sepulchre, P., & Scotese, C. R. (2022). Dataset of Phanerozoic continental climate and Köppen–Geiger climate classes. *Data in Brief*, *43*, 108424. https://doi.org/https://doi.org/10.1016/j.dib.2022.108424

Poulter, B., Ciais, P., Hodson, E., Lischke, H., Maignan, F., Plummer, S., & Zimmermann, N. E. (2011). Plant functional type mapping for earth system models. *Geoscientific Model Development*, *4*(4), 993–1010. https://doi.org/10.5194/gmd-4-993-2011

Pound, M. J., Haywood, A. M., Salzmann, U., & Riding, J. B. (2012). Global vegetation dynamics and latitudinal temperature gradients during the Mid to Late Miocene (15.97–5.33Ma). *Earth-Science Reviews*, *112*(1), 1–22. https://doi.org/https://doi.org/10.1016/j.earscirev.2012.02.005

Prentice, I. C., Cramer, W., Harrison, S. P., Leemans, R., & al., e. (1992). A global biome model based on plant physiology and dominance, soil properties and climate. *Journal of Biogeography*, *19*(2), 117–134.

Prentice, I. C., & Webb, T. (1998). BIOME 6000: reconstructing global mid-Holocene vegetation patterns from palaeoecological records. *Journal of Biogeography*, *25*(6), 997–1005. https://doi.org/10.1046/j.1365-2699.1998.00235.x

Preston, J. C., & Sandve, S. R. (2013). Adaptation to seasonality and the winter freeze [Review]. *Frontiers in Plant Science*, *4*.

Richardson, A. D., Anderson, R. S., Arain, M. A., Barr, A. G., Bohrer, G., Chen, G. S., Chen, J. M., Ciais, P., Davis, K. J., Desai, A. R., Dietze, M. C., Dragoni, D., Garrity, S. R., Gough, C. M., Grant, R., Hollinger, D. Y., Margolis, H. A.,

https://doi.org/10.5194/egusphere-2026-4262
Preprint. Discussion started: 31 August 2026

McCaughey, H., Migliavacca, M.,…Xue, Y. K. (2012). Terrestrial biosphere models need better representation of vegetation phenology: results from the North American Carbon Program Site Synthesis [Article]. *Global Change Biology*, *18*(2), 566–584. https://doi.org/10.1111/j.1365-2486.2011.02562.x

Rosenblatt, M. (1956). Remarks on Some Nonparametric Estimates of a Density Function. *The Annals of Mathematical Statistics*, *27*(3), 832 – 837. https://doi.org/https://doi.org/10.1214/aoms/1177728190

Rothwell, G. W., Stockey, R. A., & Smith, S. Y. (2020). Revisiting the Late Cretaceous Parataxodium wigginsii flora from the North Slope of Alaska, a high-latitude temperate forest. *Cretaceous Research*, *116*, 104592. https://doi.org/https://doi.org/10.1016/j.cretres.2020.104592

Rubel, F., & Kottek, M. (2010). Observed and projected climate shifts 1901-2100 depicted by world maps of the Koppen-Geiger climate classification. *Meteorologische Zeitschrift*, *19*(2), 135–141. https://doi.org/10.1127/0941-2948/2010/0430

Saatchi, S. S., & Favrichon, S. (2023). *Global Vegetation Height Metrics from GEDI and ICESat2 (Version 1)* (Version Date Accessed:). https://doi.org/https://doi.org/10.3334/ORNLDAAC/2294

Sage, R. F. (2001). Environmental and evolutionary preconditions for the origin and diversification of the C4 photosynthetic syndrome. *Plant Biology*, *3*(3), 202–213.

Saward, S. A. (1992). A global view of Cretaceous vegetation patterns. In P. J. McCabe & J. T. Parrish (Eds.), *Controls on the Distribution and Quality of Cretaceous Coals* (Vol. 267, pp. 0). Geological Society of America. https://doi.org/10.1130/SPE267-p17

Schaaf, C. B., Gao, F., Strahler, A. H., & al., e. (2002). First operational BRDF, albedo nadir reflectance products from MODIS. *Remote Sensing of Environment*, *83*(1-2), 135–148. https://doi.org/https://doi.org/10.1016/S0034-4257(02)00091-3

Schmidt, G. A., Ruedy, R., Hansen, J. E., Aleinov, I., Bell, N., Bauer, M., Bauer, S., Cairns, B., Canuto, V., Cheng, Y., Genio, A. D., Faluvegi, G., Friend, A. D., Hall, T. M., Hu, Y., Kelley, M., N.Y. Kiang, D. K., Lacis, A. A., Lerner, J.,…Yao, M.-S. (2006). Present day atmospheric simulations using GISS ModelE: Comparison to in-situ, satellite and reanalysis data. *Journal of Climate*, *19*, 153–192, . https://doi.org/https://doi.org/10.1175/JCLI3612.1

Schneider, U., Becker, A., Finger, P., Meyer-Christoffer, A., Rudolf, B., & Ziese, M. (2011). *GPCC Full Data Reanalysis Version 6.0 at 0.5°: Monthly Land-Surface Precipitation from Rain-Gauges built on GTS-based and Historic Data.* (Global Precipitation Climatology Centre, National Oceanic and Atmospheric Administration. https://doi.org/DOI: 10.5676/DWD_GPCC/FD_M_V7_050

Scotese, C., & Wright, N. (2018). *PALEOMAP Paleodigital Elevation Models (PaleoDEMS) for the Phanerozoic* (Version Version v2).

Scott, D. W. (1979). OPTIMAL AND DATA-BASED HISTOGRAMS [Article]. *Biometrika*, *66*(3), 605–610. https://doi.org/10.1093/biomet/66.3.605

Sewall, J. O., Sloan, L. C., Huber, M., & Wing, S. (2000). Climate sensitivity to changes in land surface characteristics. *Global and Planetary Change*, *26*(4), 445–465. https://doi.org/https://doi.org/10.1016/S0921-8181(00)00056-4

Sewall, J. O., van de Wal, R. S. W., van der Zwan, K., van Oosterhout, C., Dijkstra, H. A., & Scotese, C. R. (2007). Climate model boundary conditions for four Cretaceous time slices. *Climate of the Past*, *3*(4), 647–657. https://doi.org/10.5194/cp-3-647-2007

Sheffield, J., Goteti, G., & Wood, E. F. (2006). Development of a 50-yr high-resolution global dataset of meteorological forcings for land surface modeling. *Journal of Climate*, *19*(13), 3088–3111.

Shellito, C. J., & Sloan, L. C. (2006a). Reconstructing a lost Eocene Paradise, Part II: On the utility of dynamic global vegetation models in pre-Quaternary climate studies. *Global and Planetary Change*, *50*(1), 18–32. https://doi.org/https://doi.org/10.1016/j.gloplacha.2005.08.002

Shellito, C. J., & Sloan, L. C. (2006b). Reconstructing a lost Eocene paradise: Part I. Simulating the change in global floral distribution at the initial Eocene thermal maximum. *Global and Planetary Change*, *50*(1), 1–17. https://doi.org/https://doi.org/10.1016/j.gloplacha.2005.08.001

Simard, M., Pinto, N., Fisher, J. B., & Baccini, A. (2011). Mapping forest canopy height globally with spaceborne lidar [Article]. *Journal of Geophysical Research-Biogeosciences*, *116*, G04021, Article G04021. https://doi.org/10.1029/2011jg001708

Sitch, S., Huntingford, C., Gedney, N., Levy, P. E., Lomas, M., Piao, S. L., Betts, R., Ciais, P., Cox, P., Friedlingstein, P., Jones, C. D., Prentice, I. C., & Woodward, F. I. (2008). Evaluation of the terrestrial carbon cycle, future plant

https://doi.org/10.5194/egusphere-2026-4262
Preprint. Discussion started: 31 August 2026

geography and climate-carbon cycle feedbacks using five Dynamic Global Vegetation Models (DGVMs) [Review]. *Global Change Biology*, *14*(9), 2015–2039. https://doi.org/10.1111/j.1365-2486.2008.01626.x

Sitch, S., O'Sullivan, M., Robertson, E., Friedlingstein, P., Albergel, C., Anthoni, P., Arneth, A., Arora, V. K., Bastos, A., Bastrikov, V., Bellouin, N., Canadell, J. G., Chini, L., Ciais, P., Falk, S., Harris, I., Hurtt, G., Ito, A., Jain, A. K.,…Zaehle, S. (2024). Trends and Drivers of Terrestrial Sources and Sinks of Carbon Dioxide: An Overview of the TRENDY Project. *Global Biogeochemical Cycles*, *38*(7), e2024GB008102. https://doi.org/https://doi.org/10.1029/2024GB008102

Song, X., Wang, D.-Y., Li, F., & Zeng, X.-D. (2021). Evaluating the performance of CMIP6 Earth system models in simulating global vegetation structure and distribution. *Advances in Climate Change Research*, *12*(4), 584–595. https://doi.org/https://doi.org/10.1016/j.accre.2021.06.008

Spawn, S. A., Sullivan, C. C., Lark, T. J., & Gibbs, H. K. (2020). Harmonized global maps of above and belowground biomass carbon density in the year 2010. *Scientific Data*, *7*(1), 112. https://doi.org/10.1038/s41597-020-0444-4

Strömberg, C. A. E. (2011). Evolution of Grasses and Grassland Ecosystems. *Annual Review of Earth and Planetary Sciences*, *39*(Volume 39, 2011), 517–544. https://doi.org/https://doi.org/10.1146/annurev-earth-040809-152402

Strömberg, C. A. E., & McInerney, F. A. (2011). The Neogene transition from C₃ to C₄ grasslands in North America: assemblage analysis of fossil phytoliths. *PALEOBIOLOGY*, *37*(1), 50–71. https://doi.org/10.1666/09067.1

Tang, C. Q., Yang, Y., Momohara, A., Wang, H.-C., Luu, H. T., Li, S., Song, K., Qian, S., LePage, B., Dong, Y.-F., Han, P.-B., Ohsawa, M., Le, B. T., Tran, H. D., Dang, M. T., Peng, M.-C., & Wang, C.-Y. (2019). Forest characteristics and population structure of Glyptostrobus pensilis, a globally endangered relict species of southeastern China. *Plant Diversity*, *41*(4), 237–249. https://doi.org/https://doi.org/10.1016/j.pld.2019.06.007

Tian, Y. H., Woodcock, C. E., Wang, Y. J., Privette, J. L., Shabanov, N. V., Zhou, L. M., Zhang, Y., Buermann, W., Dong, J. R., Veikkanen, B., Hame, T., Andersson, K., Ozdogan, M., Knyazikhin, Y., & Myneni, R. B. (2002a). Multiscale analysis and validation of the MODIS LAI product - I. Uncertainty assessment. *Remote Sensing of Environment*, *83*(3), 414–431.

Tian, Y. H., Woodcock, C. E., Wang, Y. J., Privette, J. L., Shabanov, N. V., Zhou, L. M., Zhang, Y., Buermann, W., Dong, J. R., Veikkanen, B., Hame, T., Andersson, K., Ozdogan, M., Knyazikhin, Y., & Myneni, R. B. (2002b). Multiscale Analysis and Validation of the MODIS LAI Product. II. Sampling Strategy. Remote Sens. Environ., 83:431-441. *Remote Sensing of Environment*, *83*(3), 431–441.

Trewartha, G. T. (1968). *An introduction to climate*. McGraw-Hill.

Trewartha, G. T., & Horn, L. H. (1980). *An introduction to climate* (5th Edition ed.). McGraw Hill.

Tsigaridis, K., Ackerman, A. S., Aleinov, I., Chandler, M. A., Clune, T. L., Colose, C. M., Del Genio, A. D., Kelley, M., Kiang, N. Y., Leboissetier, A., Perlwitz, J. P., Ruedy, R. A., Russell, G. L., Sohl, L. E., Way, M. J., & Wolf, E. T. (2025). ROCKE-3D 2.0: An updated general circulation model for simulating the climates of rocky planets. *EGUsphere*, *2025*, 1–66. https://doi.org/10.5194/egusphere-2025-925

Vajda, V., & Bercovici, A. (2014). The global vegetation pattern across the Cretaceous–Paleogene mass extinction interval: A template for other extinction events. *Global and Planetary Change*, *122*, 29–49. https://doi.org/https://doi.org/10.1016/j.gloplacha.2014.07.014

Valjarević, A., Milanović, M., Gultepe, I., Filipović, D., & Lukić, T. (2022). Updated Trewartha climate classification with four climate change scenarios. *The Geographical Journal*, *188*(4), 506–517. https://doi.org/https://doi.org/10.1111/geoj.12458

van Bodegom, P. M., Douma, J. C., & Verheijen, L. M. (2014). A fully traits-based approach to modeling global vegetation distribution. *Proceedings of the National Academy of Sciences*, *111*(38), 13733. https://doi.org/10.1073/pnas.1304551110

Waltham, D. (2015). Milankovitch Period Uncertainties and Their Impact On Cyclostratigraphy. *Journal of Sedimentary Research*, *85*(8), 990–998. https://doi.org/10.2110/jsr.2015.66

Way, M. J., Aleinov, I., Amundsen, D. S., Chandler, M. A., Clune, T. L., Genio, A. D. D., Fujii, Y., Kelley, M., Kiang, N. Y., Sohl, L., & Tsigaridis, K. (2017). Resolving Orbital and Climate Keys of Earth and Extraterrestrial Environments with Dynamics (ROCKE-3D) 1.0: A General Circulation Model for Simulating the Climates of Rocky Planets. *Astrophysical Journal Supplement Series*, *accepted*.

https://doi.org/10.5194/egusphere-2026-4262
Preprint. Discussion started: 31 August 2026

Whittaker, R. H. (1967). Gradient Analysis of Vegetation. *Biological Reviews*, *49*, 207–264.

Widlowski, J.-L., Mio, C., Disney, M., Adams, J., Andredakis, I., Atzberger, C., Brennan, J., Busetto, L., Chelle, M., Ceccherini, G., Colombo, R., Côté, J.-F., Eenmäe, A., Essery, R., Gastellu-Etchegorry, J.-P., Gobron, N., Grau, E., Haverd, V., Homolová, L.,…Zenone, T. (2015). The fourth phase of the radiative transfer model intercomparison (RAMI) exercise: Actual canopy scenarios and conformity testing. *Remote Sensing of Environment*, *169*, 418–437. https://doi.org/https://doi.org/10.1016/j.rse.2015.08.016

Widlowski, J. L., Pinty, B., Clerici, M., Dai, Y., De Kauwe, M., de Ridder, K., Kallel, A., Kobayashi, H., Lavergne, T., Ni-Meister, W., Olchev, A., Quaife, T., Wang, S., Yang, W., Yang, Y., & Yuan, H. (2011). RAMI4PILPS: An intercomparison of formulations for the partitioning of solar radiation in land surface models. *Journal of Geophysical Research-Biogeosciences*, *116*(G2), Article G02019. https://doi.org/10.1029/2010jg001511

Widlowski, J. L., Pinty, B., Lopatka, M., Atzberger, C., Buzica, D., Chelle, M., Disney, M., Gastellu-Etchegorry, J. P., Gerboles, M., Gobron, N., Grau, E., Huang, H., Kallel, A., Kobayashi, H., Lewis, P. E., Qin, W., Schlerf, M., Stuckens, J., & Xie, D. (2013). The fourth radiation transfer model intercomparison (RAMI-IV): Proficiency testing of canopy reflectance models with ISO-13528. *Journal of Geophysical Research-Atmospheres*, *118*(13), 6869–6890. https://doi.org/10.1002/jgrd.50497

Wilczek, A. M., Burghardt, L. T., Cobb, A. R., Cooper, M. D., Welch, S. M., & Schmitt, J. (2010). Genetic and physiological bases for phenological responses to current and predicted climates. *Philosophical Transactions of the Royal Society B: Biological Sciences*, *365*(1555), 3129–3147. https://doi.org/10.1098/rstb.2010.0128

Willmes, C., Becker, D., Brocks, S., Hütt, C., & Bareth, G. (2017). High Resolution Köppen-Geiger Classifications of Paleoclimate Simulations. *Transactions in GIS*, *21*(1), 57–73. https://doi.org/https://doi.org/10.1111/tgis.12187

Wolfe, J. A. (1987). Late Cretaceous-Cenozoic history of deciduousness and the terminal Cretaceous event. *PALEOBIOLOGY*, *13*(2), 215–226. https://doi.org/10.1017/S0094837300008769

Wu, Y., You, H.-L., & Li, X.-Q. (2018). Dinosaur-associated Poaceae epidermis and phytoliths from the Early Cretaceous of China. *National Science Review*, *5*(5), 721–727. https://doi.org/10.1093/nsr/nwx145

Xu, X., & Chen, D. (2024). Estimating global annual gross primary production based on satellite-derived phenology and maximal carbon uptake capacity. *Environmental Research*, *252*, 119063. https://doi.org/https://doi.org/10.1016/j.envres.2024.119063

Yoo, J., & Rohli, R. V. (2016). Global distribution of Köppen–Geiger climate types during the Last Glacial Maximum, Mid-Holocene, and present. *Palaeogeography, Palaeoclimatology, Palaeoecology*, *446*, 326–337. https://doi.org/https://doi.org/10.1016/j.palaeo.2015.12.010

Zhang, L., Wang, C., Li, X., Cao, K., Song, Y., Hu, B., Lu, D., Wang, Q., Du, X., & Cao, S. (2016). A new paleoclimate classification for deep time. *Palaeogeography, Palaeoclimatology, Palaeoecology*, *443*, 98–106. https://doi.org/https://doi.org/10.1016/j.palaeo.2015.11.041

https://doi.org/10.5194/egusphere-2026-4262
Preprint. Discussion started: 31 August 2026

1068 Supplementary Material (see attached documentation, data files, and plots)

1069